



NRL/MR/7140--00-8453

# **Bottom Backscattering Measured Off the Coast of Oregon During the Littoral Warfare Advanced Development 99-3 Experiment**

EDWARD L. KUNZ

ROGER C. GAUSS

*Acoustic Systems Branch*

*Acoustics Division*

June 12, 2000

20000608 072

Approved for public release; distribution unlimited.

REPORT DOCUMENTATION PAGE			Form Approved OMB No. 0704-0188	
Public reporting burden for this collection of information is estimated to average 1 hour per response, including the time for reviewing instructions, searching existing data sources, gathering and maintaining the data needed, and completing and reviewing the collection of information. Send comments regarding this burden estimate or any other aspect of this collection of information, including suggestions for reducing this burden, to Washington Headquarters Services, Directorate for Information Operations and Reports, 1215 Jefferson Davis Highway, Suite 1204, Arlington, VA 22202-4302, and to the Office of Management and Budget, Paperwork Reduction Project (0704-0188), Washington, DC 20503.				
1. AGENCY USE ONLY (Leave Blank)		2. REPORT DATE June 12, 2000	3. REPORT TYPE AND DATES COVERED Interim Report October 1999 to May 2000	
4. TITLE AND SUBTITLE Bottom Backscattering Measured Off the Coast of Oregon During the Littoral Warfare Advanced Development 99-3 Experiment			5. FUNDING NUMBERS PE-0603747N PE-62435N	
6. AUTHOR(S) Edward L. Kunz and Roger C. Gauss				
7. PERFORMING ORGANIZATION NAME(S) AND ADDRESS(ES) Naval Research Laboratory Washington, DC 20375-5320			8. PERFORMING ORGANIZATION REPORT NUMBER NRL/MR/7140--00-8453	
9. SPONSORING/MONITORING AGENCY NAME(S) AND ADDRESS(ES) Office of Naval Research 800 North Quincy Street Arlington, VA 22217-5660			10. SPONSORING/MONITORING AGENCY REPORT NUMBER	
11. SUPPLEMENTARY NOTES				
12a. DISTRIBUTION/AVAILABILITY STATEMENT Approved for public release; distribution unlimited.			12b. DISTRIBUTION CODE	
13. ABSTRACT (Maximum 200 words)  Measurements of backscattering from the ocean bottom were performed in a shallow water environment off the coast of Oregon as part of the Littoral Warfare Advanced Development 99-3 Experiment. Scattering strengths were obtained at 0.4 to 4.5 kHz as a function of the mean grazing angle. For all measurements, the grazing angle dependence was fit adequately by assuming a dependence of scattering strength (dB) on the sine of the mean grazing angle: $\mu + 10 \log(\sin \theta)$ . At the primary scattering location (Site 1), most scattering strengths were well fit using $\mu = -25$ to $-30$ dB at low frequencies (400-1000 Hz), and $\mu = -20$ to $-30$ dB at mid frequencies (1.5-4.5 kHz). Application of physics-based, bistatic models suggest that the dominant scattering mechanisms at grazing angles below $\sim 50$ deg were the water-sediment interface and near-bottom fish.				
14. SUBJECT TERMS Bottom scattering      Active sonar Reverberation      Underwater acoustics Volume scattering			15. NUMBER OF PAGES 34	
			16. PRICE CODE	
17. SECURITY CLASSIFICATION OF REPORT UNCLASSIFIED	18. SECURITY CLASSIFICATION OF THIS PAGE UNCLASSIFIED	19. SECURITY CLASSIFICATION OF ABSTRACT UNCLASSIFIED	20. LIMITATION OF ABSTRACT UL	

## CONTENTS

INTRODUCTION . . . . .	1
TEST OPERATIONS . . . . .	2
Test Location . . . . .	2
Measurement Overview . . . . .	3
DATA PROCESSING . . . . .	3
MEASURED BACKSCATTERING STRENGTHS . . . . .	4
LF Site-1 Measurements . . . . .	4
MF Site-1 Measurements . . . . .	5
Drifting Site Measurement . . . . .	6
MODELING . . . . .	6
Model Overview . . . . .	6
Bottom-Scattering Model Inputs . . . . .	7
Fish-Scattering Model Inputs . . . . .	8
Bottom Parameters . . . . .	8
Fish Parameters . . . . .	8
Parameter Sensitivity . . . . .	9
Discussion . . . . .	9
Modeled Backscattering Strengths . . . . .	10
LF Results . . . . .	10
MF Results . . . . .	11
Comments . . . . .	11
SUMMARY . . . . .	12
ACKNOWLEDGMENTS . . . . .	13
REFERENCES . . . . .	13

# BOTTOM BACKSCATTERING MEASURED OFF THE COAST OF OREGON DURING THE LITTORAL WARFARE ADVANCED DEVELOPMENT 99-3 EXPERIMENT

## INTRODUCTION

For operational active sonars, scattering from the ocean boundaries and biologics, coupled with propagation conditions, can severely limit the detectability of returns from features of interest. Furthermore, reverberation limits can vary dramatically, depending on the local geology, oceanography and biology. Hence, accurately predicting the impact of the environment on active sonar performance will depend not only on finding suitable empirical or physics-based models that describe the scattering and propagation, but also on acquiring the necessary inputs to those models.

In particular, the bottom interaction problem can involve multiple physical processes, all of which may contribute to the measured scattering strength: scattering from the water/sediment interface, scattering in the sediment volume itself, or scattering from the basement or subsurface layers with a significant impedance mismatch. (Additionally, fish in the vicinity of the bottom can be a subtle and competing scattering mechanism.) Furthermore, given the typical variability of the littoral environment in sediment thickness, composition, and frequency-dependent attenuation, correct physical interpretation of bottom scattering strengths (BSS) usually requires significant knowledge of the geoacoustic properties and structure of the subbottom. (For example, regions where a thin sediment layer overlies a bathymetrically-varying substrate can exhibit greater variability in frequency and site dependence; in this case, the results will depend on specific, range-dependent characteristics such as sediment layer thickness.)

While BSS in general has a complex dependence on frequency, scattering angle, and bottom properties, one can begin to separate out the different potential scattering mechanisms by making measurements at a given site over a wide range of frequencies and scattering angles. This approach was employed during the LWAD-99-3 bottom backscattering measurements, the seventh in a series of such LWAD measurements<sup>1</sup>, where the LWAD BSS measurement technique was extended in two significant ways:

- Expanding the frequency coverage down to 400 Hz by adding a lower-frequency source and matching receiver aperture. The frequency coverage is now 400-5000 Hz, covering not only a broad spectrum of frequencies of potential interest to the Navy, but increased physical insight into the scattering mechanisms.

---

Manuscript approved May 19, 2000.

<sup>1</sup>Focused Technology Experiment 96-2 (FTE 96-2), Focused Technology Experiment 97-2 (FTE 97-2), System Concept Validation 97 (SCV-97), LWAD Experiment 98-2 (LWAD 98-2), LWAD Experiment 98-4 (LWAD 98-4) and LWAD Experiment 99-1 (LWAD 99-1). The FTE 96-2, SCV-97 and LWAD 98-4 backscattering measurements were made off the Carolina coast and the results appear in [1,2,3]. The FTE 97-2, LWAD 98-2 and LWAD 99-1 measurements were made off the western coast of Florida and the results are reported in [4,5,6].

- Conducting vertically-bistatic measurements via repeated measurements at a given site with different source-receiver separations. The additional information is important in validating models that are used to predict multistatic active sonar performance.

This report details the results of broadband, bistatic, direct-path measurements of bottom backscattering strength made during the Littoral Warfare Advanced Development (LWAD) 99-3 experiment. We begin with a summary of the data collection and analysis approach. This is followed by a discussion of the acoustic measurement results (including empirical modeling results). BSS data were obtained at frequencies from 0.4 to 5 kHz for grazing angles of 4 to 40 degrees. Next, physics-based modeling results are presented which suggest that the dominant scattering mechanisms responsible for the observed BSS's are the water-sediment interface and near-bottom fish. We conclude with a summary of key results.

## TEST OPERATIONS

The LWAD 99-3, direct-path bottom scattering tests were conducted in shallow water off the Oregon coast, at the head of Perpetua Bank, over a one-week period in September 1999. The measurements were made in two frequency bands, each using a vertical line array receiver and a transducer deployed on a single cable from the research vessel (R/V) *NEW HORIZON*.

### Test Location

Six bottom scattering measurements (Runs 1-6) were conducted while the R/V *NEW HORIZON* was moored at Site 1 (mean location: 44.32° N 124.67° W). The water depths at this site ranged from 82 to 93 m (mean 91 m) as the vessel moved about the moor. A bottom grab taken near Site 1 revealed mudstone with some gravel.

A seventh bottom scattering measurement (Run 7) was conducted while drifting 14 km west of Site 1. As the vessel drifted south, the water depth decreased from 174 to 160 m. A bottom grab taken near the drifting site revealed a mix of clay and silt.

Table 1 shows the date and time in Zulu (Z) and location for the seven bottom backscattering runs. Figure 1 shows the location of the mooring site (Site 1) as the solid circle and the drifting site as the straight vertical line.

Table 1 — LWAD 99-3 Bottom Scattering Runs

Run #	Date (Z)	Time (Z)	Site	Site Location
1	12 Sep 1999	11:19 - 12:51	Site 1	44.31° N 124.67° W
2	13 Sep 1999	01:15 - 02:06	Site 1	44.31° N 124.66° W
3	13 Sep 1999	16:58 - 21:45	Site 1	44.32° N 124.66° W
4	14 Sep 1999	07:24 - 10:07	Site 1	44.32° N 124.66° W
5	14 Sep 1999	22:29 - 23:59	Site 1	44.32° N 124.66° W
6	16 Sep 1999	18:20 - 21:27	Site 1	44.31° N 124.67° W
7	17 Sep 1999	10:26 - 10:45	Drifting Site	44.29° N 124.84° W

## Measurement Overview

Receiver Characteristics. A vertical line array (VLA) was used with two apertures: a low-frequency (LF) aperture consisting of 16 elements uniformly spaced at 30 inches (0.76 m); and a mid-frequency (MF) aperture consisting of 16 elements uniformly spaced at 6 inches (0.15 m). The LF aperture received acoustic data in the 400- to 1000-Hz range, while the MF aperture received data in the 1.5- to 4.5-kHz range.

Source Characteristics. The LF source was a transducer (XF4) usable over 300 to 1000 Hz and resonant at 400 Hz. It has a maximum source level of 203 dB *re*  $(1\mu\text{Pa})^2/\text{Hz}$  at 1 m at resonance (400 Hz) that decreases with increasing frequency to 194 dB at 600 Hz, 193 dB at 800 Hz, and 191 dB at 1000 Hz. The MF source was a USRD ring-shaped transducer (G81) usable over 1-5 kHz and resonant at 3 kHz. It has a maximum source level of 198 dB *re*  $(1\mu\text{Pa})^2/\text{Hz}$  at 1 m at resonance (3 kHz) that decreases with both decreasing and increasing frequency to 189 dB at both 1.5 and 5 kHz.

Waveforms. For both the LF and MF measurements, the transmitted waveforms were 50-ms gated continuous wave (GCW) signals and 200-ms linear frequency modulated (LFM) signals.

At LF, 20 identical wavetrains consisting of four adjacent GCW signals were transmitted in the sequence 400, 800, 600, and 1000 Hz. Additionally, LFM signals sweeping 400-1000 Hz were transmitted. At MF, two sets of 20 identical wavetrains consisting of four adjacent GCW signals were transmitted: one set consisted of signals in the sequence 1, 2, 1.5, and 2.5 kHz; the second set consisted of signals in the sequence 3, 4, 3.5, and 4.5 kHz. Additionally, LFM signals, one sweeping 1 to 3 kHz and one sweeping 3 to 5 kHz, were transmitted. At both LF and MF, the wavetrains were separated by 15 s.

Measurement Geometries. For most of the bottom scattering runs at Site 1, the source was deployed at a depth of approximately 36 m, 4 m above the center of the MF aperture and 8 m above the center of the LF aperture. This produced a nearly monostatic measurement geometry, with the scattered (receiver) angle  $\theta_{\text{scat}}$  approximately equal to 0.9 times the incident (source) angle  $\theta_{\text{inc}}$ . In addition to the near-monostatic data collection, vertically-bistatic LF and MF measurements were made in which the source and receiver were separated vertically by 25 to 30 m ( $\theta_{\text{scat}} \approx 0.6\theta_{\text{inc}}$ ) and 50 to 55 m ( $\theta_{\text{scat}} \approx 0.25\theta_{\text{inc}}$ ).

At the drifting site, the source was deployed at a depth of approximately 78 m, 8 m above the center of the LF aperture.

## DATA PROCESSING

The bottom reverberation from the signals was received<sup>2</sup> on the VLA. Seventeen, spatially-Hanned beams with cosine-spaced main response axes (MRAs) were formed for each of the two 16-phone apertures, with most of the usable returns coming from the downward-looking beams closest to broadside.

After beamforming, reverberation time series curves were obtained for individual GCW pings

<sup>2</sup>The system calibration was computed to within 1 dB accuracy.

using spectral processing, while the individual LFM pings were matched filtered. For the GCW ping data, a uniform window matched to the signal duration (50 ms) was slid over the length of each beam time series with a 50%-overlap. The resulting time series segments were then Fourier transformed to obtain power spectra, with reverberation level computed by integrating the total received signal power over a narrow frequency band (50 Hz) centered on the frequency of the transmitted signal. For each set of GCW and LFM data, the 20 individual pings were temporally aligned with respect to signal transmit time and then linearly averaged to produce a single reverberation curve for each beam.

A raytrace program was then used to calculate the geometric effects unique to each measurement: (1) calculating geometric spreading loss along each ray path, the transmission loss terms to and from the scattering patch were obtained; and (2) using the computed beam patterns and raytraces, the scattering patch areas were obtained.

Finally, the average reverberation curves were combined with these geometric parameters and source level to solve the sonar equation for backscattering strength as a function of frequency, beam, and grazing angles:

$$BSS = RL - SL + TL_s + TL_r - 10 \log A \quad (1)$$

where  $BSS$  is the scattering strength in dB,  $RL$  is the measured reverberation level in dB *re*  $(1\mu\text{Pa})^2/\text{Hz}$ ,  $SL$  is the source level in dB *re*  $(1\mu\text{Pa})^2/\text{Hz}$  at 1 m,  $TL_s$  is the transmission loss from the source to the ensonified patch on the bottom in dB,  $TL_r$  is the transmission loss from the ensonified patch on the bottom to the receiver in dB, and  $A$  is the area of the ensonified patch in  $\text{m}^2$ .

## MEASURED BACKSCATTERING STRENGTHS

Backscattering strengths as a function of mean grazing angle measured during LWAD 99-3 are shown in Figs. 2 to 19. In each case,  $BSS$  is plotted vs. the mean of the incident and scattered grazing angles.<sup>3</sup> In each case, the plotted  $BSS$  values represent returns from beams whose MRAs spanned 60 to 83 degrees relative to bottom endfire (linearly averaged where appropriate, i.e. where there was grazing-angle overlap).

The standard deviations due to ping-to-ping variability within the sets of identical transmissions were  $\pm 2$  to 3 dB.

### LF Site-1 Measurements

Near-monostatic Measurements. Figure 2 shows near-monostatic ( $\theta_{\text{scat}} \approx 0.9\theta_{\text{inc}}$ ) backscattering strengths measured using 400-Hz GCWs as a function of mean grazing angle. The solid curve represents a (linear) average over six separate measurements at Site 1. The dashed curves represent  $\mu + 10 \log(\sin \theta)$  dB for  $\mu = -25, -27.5$ , and  $-30$ . These curves show that the grazing angle dependence can be fit adequately by assuming a first-power-law dependence of scattering strength on the sine of the mean grazing angle.

<sup>3</sup>For the bulk of the cases, the source-receiver geometries are nearly monostatic with  $\theta_{\text{scat}} \approx 0.9\theta_{\text{inc}}$ , so that using the average of these two angles ( $\equiv \theta$ ) provides a reasonable approximation.

Figures 3 to 5 present near-monostatic GCW backscattering results for the remaining three frequencies in the LF band (600, 800, and 1000 Hz) averaged over eight separate measurements at Site 1. Figure 6 overlays the BSS curves presented in Figs. 2 to 5. The thin solid curve in Fig. 6 is the Mackenzie curve:  $-27 + 10\log(\sin^2 \theta)$  dB, a reference curve showing Lambert's law with a coefficient of -27 dB. This formula is the standard input to Navy performance models, with the selection of the -27 dB value originating in the work of Mackenzie [7].

Figure 7 shows the backscattering strength measured using low-frequency LFM (400-1000 Hz) as a function of mean grazing angle. The solid curve represents a (linear) average over four separate near-monostatic measurements at Site 1. The dashed curves represent  $\mu + 10\log(\sin \theta)$  dB for  $\mu = -25, -27.5$  and  $-30$ . Figure 8 overlays this LFM BSS curve with an average GCW BSS curve, the (linear) average of the four data curves of Fig. 6. As is to be expected, the agreement of the two curves is excellent (as scattering strength, a mean quantity, is independent of waveform for almost all scatterers).<sup>4</sup> The dashed curves represent  $\mu + 10\log(\sin \theta)$  dB for  $\mu = -25, -27.5$  and  $-30$ .

The near-monostatic LF backscattering strength measurements cover mean grazing angles from 4 to 40 degrees and can be fit by  $\mu + 10\log(\sin \theta)$  using proportionality constants  $\mu$  in the range of -25 to -30 dB. The bottom material at Site 1 falls on the boundary between Group 1 (rock, coarse sand, shell) and Group 2 (fine sand, silt) of McCammon's three-group model for bottom backscattering strengths [8]. Groups 1 and 2 have average  $\mu$  values of  $-18.7 \pm 8.6$  dB and  $-27.5 \pm 6.8$  dB, respectively [8]. These LF LWAD 99-3 scattering strengths align best with those of Group 2.

Vertically-bistatic Measurements. Figure 9 shows backscattering strengths measured using GCWs as a function of mean grazing angle for a vertically-bistatic ( $\theta_{\text{scat}} \approx 0.6 \cdot \theta_{\text{inc}}$ ) geometry during Run 6 (frequencies: 400, 600, 800, and 1000 Hz). The source (21-m depth) and receiver (51-m depth) were separated by 30 m. The dashed curves represent  $\mu + 10\log(\sin \theta)$  dB for  $\mu = -25, -27.5$  and  $-30$ . In this case, the measured BSS's are in general agreement with the near-monostatic results (cf. Fig. 6). This is not surprising as the average angle  $\theta$  ( $\approx 0.8 \cdot \theta_{\text{inc}}$ ) still provides a reasonable approximation.

Figure 10 shows backscattering strengths measured using the four GCW signals as a function of mean grazing angle for a more vertically-bistatic ( $\theta_{\text{scat}} \approx 0.2 \cdot \theta_{\text{inc}}$ ) measurement during Run 6, with the source (21-m depth) and receiver (76-m depth) now separated by 55 m. The dashed curves represent  $\mu + 10\log(\sin \theta)$  dB for  $\mu = -25, -30$  and  $-35$ . In this case, the measured BSS's are noticeably lower than the less vertically-bistatic results (cf. Figs. 6 and 9), and generally only follow the empirical formula below 10 deg grazing. (Using the bistatic form of  $\mu + 10\log(\sin \theta)$  did little to improve the fit.)

## MF Site-1 Measurements

Figures 11 to 17 present MF backscattering strengths as a function of mean grazing angle. In each case, the solid curve represents a (linear) average of three near-monostatic GCW measurements at Site 1 (frequencies: 1.5, 2, 2.5, 3, 3.5, 4, and 4.5 kHz). The dashed curves represent  $\mu + 10\log(\sin \theta)$  dB for  $\mu = -20, -25$ , and  $-30$ . Figure 18 overlays the seven BSS curves presented in Figs. 11 to 17. For reference, the Navy-standard Mackenzie curve is also shown.

<sup>4</sup>Similar agreement between BSS curves derived from LFM and GCW transmissions was seen at MF.

The near-monostatic MF backscattering strength measurements cover mean grazing angles of 4 to 36 degrees and can be fit by  $\mu + 10 \log(\sin \theta)$  with  $\mu$  in the range of -20 to -30 dB. As with the LF bottom-scattering results, the MF results are closest to lying within McCammon's Group 2 [8].

### Drifting Site Measurement

Figure 19 shows the near-monostatic backscattering strengths measured at the drifting site (14 km west of Site 1) using the LF GCWs (frequencies: 400, 600, 800, and 1000 Hz). The data cover mean grazing angles of 20 to 30 degrees.

During this single measurement, there was excessive array tilt due to high currents. Array tilt violated the azimuthal symmetry of the measurement and hence the results may be inaccurate. (The array tilt also limited grazing angle coverage.) The backscattering data from the drifting site are presented here with this caveat.

### MODELING

To gain some insight into the acoustic data results, estimates of the backscattering contributions of the ocean bottom interface as well as the expected dominant low-frequency fish were made using two physics-based, bistatic scattering strength models recently developed at NRL [9].

The motivation for including fish-scattering modeling comes from the quick-look assessment of volume (fish) scattering during LWAD 99-3 by Charles Thompson of NRL [10]. His preliminary analysis of one LF nighttime measurement, Event 63G, yielded fairly high volume scattering strengths of -32 to -36 dB over 400 to 1000 Hz. He further identified that the dominant LF fish scatterers at Site 1 were most likely rockfish. That these numbers are in the general range of the measured LF scattering strengths (Figs. 6 to 8), suggests that scattering from rockfish must be considered in modeling the LF LWAD 99-3 bottom backscattering data results.<sup>5</sup>

### Model Overview

The two NRL scattering models provide estimates of the dependence of backscattering strength on the incident and scattered grazing angles, the acoustic frequency, and physical descriptors of the environment. One model describes scattering from rough bottom interfaces, while the other model describes scattering from fish in the presence of the ocean bottom.

The bottom scattering model is a physically-intuitive, small-slope approximation capable of handling rough, elastic bottoms [11]. (Scattering from the sediment volume is *not* described by this model.) One feature of this model is that it reduces to the first-order perturbation theory result in the appropriate limits.

The fish scattering model couples a boundary-interference model with a resonant fish-scattering model of Love [12] to provide estimates of scattering levels from dispersed, bladdered fish in the presence of the ocean bottom [9]. (When such fish are near an ocean boundary, interference effects

<sup>5</sup>No analysis results are yet available from the MF volume-scattering measurements, so this report restricts its attention to rockfish with the caveat that the estimates of other potential fish-scattering contributions to the measured BSS's are incomplete (in particular, at MF).

can be significant.) With this model, the total scattering from a layer of fish is simply the incoherent sum of scattering from the individuals.

### Bottom-Scattering Model Inputs

The required environmental parameters for the bottom scattering model include the sound speed in the water column at the water-sediment interface ( $c_0 \approx 1485$  m/s during the Site-1 LWAD 99-3 measurements), and:

$\rho$  = ratio of bottom mass density to water mass density

$c_p$  = complex sound speed (m/s) of the p-wave in the bottom (compressional speed and attenuation)

$c_s$  = complex sound speed (m/s) of the s-wave in the bottom (shear speed and attenuation)

$p$  = exponent of the bottom relief spectrum<sup>6</sup>

$w$  = strength of the bottom relief spectrum at wavenumber  $2\pi/\lambda$ .

Inputs for the first three listed parameters should derive from their average values in the upper  $\sim \lambda$  of the bottom.

For the location of these scattering tests (Site 1), James Fulford of NRL has provided a geophysical description [14]. Fulford describes the material at this site as a "well consolidated, diatomaceous silty claystone characterized by a rough surface". He has provided the following values for input into the NRL model: density ratio = 2.2; compressional speed = 2300 m/s; compressional attenuation = 0.02 dB/m/kHz; shear speed = 800 to 900 m/s; and shear attenuation = 0.07 dB/m/kHz. Unfortunately, surface roughness was unable to be quantified due to the apparent pitch and roll of the survey vessel. Consequently, after first setting  $\rho$ ,  $c_p$ , and  $c_s$  to the above values (using a 5-point average over 800-900 m/s to fix the shear speed), the remaining two bottom parameters were fixed by fitting the NRL model to the acoustic data:  $p = 3.5$  and  $w = 0.002$ .

With these geophysical values, there will be a p-wave critical angle at  $\sim 50$  deg, and no s-wave critical angle. Typically, below the critical angle, interface scattering dominates the bottom contribution. Further, as the bottom supports shear, elastic effects can be significant. As all the Site-1 acoustic data correspond to sub-critical grazing angles (Figs. 1 to 18), using a model that predicts bistatic scattering from rough, elastic interfaces should provide a reasonable estimate of the scattering contribution from the ocean bottom (given the above geophysical inputs).

Below the critical angle, model predictions of BSS were relatively insensitive to modest changes in most of the input parameters. Exceptions are the strength of the bottom relief spectrum  $w$  and the shear speed. Changes in  $w$  affect primarily BSS level, while changes in the shear speed affect both BSS level and grazing-angle behavior. For example, keeping all the other parameters as above, increasing  $w$  from 0.002 to 0.006 increases BSS levels by  $\sim 4$  dB, whereas decreasing the shear speed by 10% of its mean value to 685 m/s, moves a null in grazing angle from 40 deg to 30 deg and decreases BSS levels below this angle by  $\sim 5$  dB. (In contrast, increasing the shear speed by the same percentage had a relatively modest effect on the BSS levels and grazing angle dependence.)

<sup>6</sup>In this model the surface roughness is considered to be a random process, described by a two-parameter, isotropic, two-dimensional roughness spectral density of the form  $W(K) = w/(h_0 K)^p$ , where  $K$  is the magnitude of the two-dimensional wave vector and  $h_0$  is a reference length to balance dimensions in the equation [13]. It is assigned the value 1.

## Fish-Scattering Model Inputs

The fish-scattering model requires environmental parameters for both the fish and bottom [9]. The latter parameters are required to properly account for boundary-interference effects when a layer of fish lies between the sonar and the boundary, as is expected to be the case with rockfish in the Site-1, bottom-backscattering source-receiver geometries [10].

### Bottom Parameters

The required bottom parameters are  $\rho$ ,  $c_0$ , and  $c_p$ . Their assumed values are as above.

### Fish Parameters

The backscattered level from a layer of dispersed fish depends primarily on their sizes, densities, and depths. Thompson *et al.* [15] provides estimates of these and other<sup>7</sup> required model inputs for the varieties of shoaling rockfish in the vicinity of Perpetua Bank:

**Sizes.** At low to mid frequency, sound scatters primarily from the fish's swimbladder, typically occupying ~3-5% of a fish's volume [12]. Hence, for modeling the key size parameter of interest is swimbladder size. Fish-size distributions are usually given as distributions of total length  $L$ . However, length-volume-weight relations are available for many fish, and they can be used to determine swimbladder size directly [12]. In the case of the Site-1 rockfish, a representative size distribution is given as [15]: 50% small rockfish,  $L = 0.15 \text{ m} \pm 33\%$ ; 40% medium-size rockfish,  $L = 0.25 \text{ m} \pm 40\%$ ; and 10% large rockfish,  $L = 0.40 \text{ m} \pm 50\%$ . For all these rockfish, swimbladder radii are assumed to be given by  $0.055 \cdot L$ .

**Densities.** The types and abundances of rockfish within the LWAD 99-3 experimental area are expected to be highly variable from site to site, with layer densities ranging from very low values to as high as  $1.4 \text{ fish/m}^2$ . For Site 1, an average layer density of  $0.09 \text{ fish/m}^2$  is assumed for the aggregate of small, medium-size and large rockfish.

**Depths.** The rockfish are assumed to be generally in the lower 40% of the water column during the day and spreading out over the lower 60% of the water column at night. A mean water depth for the Site-1 scattering measurements was 91 m, so that representative rockfish depths would then be 55 to 91 m during the day, and 36 to 91 m at night. As the measured BSS's represent averages over a number of (both day and night) measurements, for all our model runs the rockfish were assumed to be uniformly distributed over depths of 45 to 91 m.

In general, the fish contributing to the observed backscatter during these measurements will be a function of grazing angle and frequency as the water-column scatterers contributing at a given time will be those within the intersection of the receiver beam with the equi-time ellipse associated with the grazing angle at the water-sediment interface: at earlier times (higher grazing angles), steeper-looking beams will see backscatter from fish at deeper depths than at later times (lower grazing angles), when more of the assumed fish layer of 45 to 91 m will be contributing. Additionally, the (3-dB-down) beamwidths are frequency dependent as the LF and MF VLAs were cut for 1

<sup>7</sup>Other biological settings include: density of fish flesh =  $1050 \text{ kg/m}^3$  and the viscosity of fish flesh =  $50 \text{ Pa-s}$  [12]. It was also assumed that the rockfish swimbladders do not compress with depth [15].

and 5 kHz, respectively. (For example, a beam that has a 10-deg beamwidth at 4.5 kHz will have beamwidths of 13, 18 and 30 deg at 3.5, 2.5 and 1.5 kHz, respectively.) The combination of these effects means that the fish in the layer 0 to  $\sim H_{fish} \equiv R \cot \theta_{scat} \sin(\beta/2)$  m above the bottom will be the ones contributing to the BSS, where  $R$  is the distance from the bottom to the VLA in m,  $\beta$  is the beamwidth in deg and  $H_{fish} \leq R$ .<sup>8</sup>

For this report, our modeling approximates this grazing-angle dependence by assuming  $H_{fish}$  to be constant over four distinct angular regions: for  $\theta_{scat} < \sim 13$  deg, it is assumed the full fish layer (up to the receiver depth off the bottom) will contribute at each frequency; while for  $\sim 13 < \theta_{scat} < 20$  deg,  $20 < \theta_{scat} < 30$  deg, and  $\theta_{scat} > 30$  deg, only frequency-dependent fractions of the full layer (up to the receiver depth off the bottom) will contribute. Accordingly, the corresponding fish densities were reduced proportionally.

### Parameter Sensitivity

The fish-scattering model results were relatively insensitive to modest changes in most of the input parameters. An exception is the density (= layer density/layer depth), to which the backscattering strength is proportional. (For example, doubling the density increases the backscattering strength by 3 dB at all frequencies and angles.)

### Discussion

When a layer of fish lies between the sonar and a boundary, boundary-interference effects can be significant [9]. Figures 20 and 21 provide an estimate of their significance at Site 1 during the LWAD 99-3 scattering measurements.

Figure 20 plots the relative effects of including a bottom in the fish modeling. Plotted are the predicted differences in rockfish backscattering strength with and without a bottom as a function of grazing angle, for a monostatic ( $\theta_{scat} = \theta_{inc}$ ) geometry at four frequencies (assuming the above bottom and fish parameters). It is seen that bottom-interference effects can be significant, typically enhancing the backscattering strength below the p-wave critical angle of 50 deg by:  $\sim 4$  dB when the full fish layer is contributing ( $\theta < \sim 13$  deg), and by somewhat smaller levels when less than the full fish layer is contributing ( $\theta > \sim 13$  deg). Above the critical angle, there is bottom penetration and the differences (in this case) generally become negative. An exception is at 400 Hz, where the enhancement is roughly 3 dB greater at all angles than at the other LF frequencies. This is primarily due to a downward shift in the rockfish resonance pattern as seen in the next figure.

Figure 21 shows the frequency dependence of monostatic, rockfish backscattering strength at a nominal low grazing angle of 10 deg. The solid curve is the model prediction which includes bottom-interference effects, while the dashed curve is the model prediction assuming no bottom. In addition to the aforementioned resonance shift, it is seen that above resonance, in the geometric scattering region, there is a significant predicted enhancement (up to 8 dB) in backscattering strength at low angles due to presence of the claystone bottom.

<sup>8</sup>Most of the scattering geometries had the midpoint of the receiver aperture near the top of this 46-m-thick model layer. An exception was the most vertically-bistatic geometry which had the source well above this layer, but the VLA in the midst of this layer. In this case, only the bottom third of the fish layer was potentially contributing to the measured BSS.

In general, the significance of the bottom to the acoustics will depend on a variety of factors such as the sonar geometry, fish characteristics and behavior, and bottom composition.

### Modeled Backscattering Strengths

Model predictions were generated primarily for the Site-1, near-monostatic, LF (MF) scattering measurements, i.e. where the mean receiver depths were 8 (4) m lower than the source depths. Additionally, two sets of LF vertically-bistatic predictions were generated corresponding to when the source-receiver separation was increased from 8 m to 30 m, and then from 30 to 55 m, during Run 6.

Figure 22 displays predictions of the relative contributions of the water-sediment interface and rockfish to backscattering strength as a function of frequency for 3 mean grazing angles. (These bistatic predictions correspond to the near-monostatic cases, i.e. where  $\theta_{scat} \approx 0.9 \cdot \theta_{inc}$ .) It can be seen that at 30 deg, scattering from the bottom interface dominates except near a couple of the rockfish resonance frequencies ( $\sim 150$ -600 Hz). (The jump at 1 kHz reflects the switch in apertures from LF to MF.) As the grazing angle gets lower (until  $\sim 10$  deg), the rockfish contributions to BSS increase as more of the fish layer is ensonified. At 10 deg, rockfish scattering is the stronger contributor over  $\sim 100$ -1200 Hz, while bottom scattering is the stronger contributor elsewhere. At 5 deg, rockfish scattering dominates over 100 to 5000 Hz, with bottom scattering of significance only below  $\sim 100$  Hz.

Figures 23 to 30 present pairs of predictions of backscattering strength as a function of mean grazing angle: Figs. 23 to 28 correspond to three different vertically-bistatic LF scattering geometries, while Figs. 29 and 30 correspond to a near-monostatic MF scattering geometry. In each plot, four curves are shown that represent narrowband predictions at the indicated frequencies. For each plot pair, the first plot presents just the backscattering contribution from the bottom interface, while the second plot includes the backscattering contributions from both the bottom interface and rockfish. Additionally, in each plot, curve(s) representing  $\mu + 10 \log(\sin^{1/2} \theta_{inc} \cdot \sin^{1/2} \theta_{scat})$  dB are included for reference.

### LF Results

Figures 23 and 24 correspond to the near-monostatic LF backscattering geometry where  $\theta_{scat} \approx 0.9 \cdot \theta_{inc}$ . Figure 23 shows a prediction of the scattering contribution due to the bottom interface. Key features include: a mild, monostatic frequency dependence; a dramatic null near 40 deg (due to shear effects); and a much more rapid falloff of BSS with decreasing grazing angle below  $\sim 20$  deg than seen in the acoustic data (cf. Fig. 6). Figure 24 shows the predicted effects of including a rockfish scattering contribution: the frequency dependence is no longer monotonic below 40 deg; the null near 40 deg is partially filled; and grazing-angle dependence at low angles now resembles that of the acoustic data (as corroborated by the thin model curve which represents a  $\mu$  of -27.5 dB).

Figures 25 and 26 correspond to the vertically-bistatic LF backscattering geometry where  $\theta_{scat} \approx 0.6 \cdot \theta_{inc}$ . Figure 25 shows a prediction of the scattering contribution due to the bottom interface, while Fig. 26 shows the predicted effects of including a rockfish scattering contribution. The results are very similar to the near-monostatic case (Figs. 23 and 24), the most noticeable

effect being a small shift in the location of the null (which is to be expected given the increasingly bistatic geometry). Again, the data trends are generally well-matched by the predictions (cf. Fig. 9) (as corroborated by the thin model curve which represents a  $\mu$  of -27.5 dB).

Figures 27 and 28 correspond to the vertically-bistatic LF backscattering geometry where  $\theta_{scat} \approx 0.2 \cdot \theta_{inc}$ . Figure 27 shows a prediction of the scattering contribution due to the bottom interface, while Fig. 28 shows the predicted effects of including a rockfish scattering contribution.<sup>9</sup> The results differ somewhat from the previous cases: besides an expected further shift in the location of the null, the curves are lower in level (again in concert with the data—cf. Fig. 10). For this plot, three  $\mu + 10 \log(\sin^{1/2} \theta_{inc} \cdot \sin^{1/2} \theta_{scat})$  curves are shown: one for a  $\mu$  of -27.5 dB, one for a  $\mu$  of -30 dB (which fit the data below 10 deg—Fig. 10), and one for a  $\mu$  of -35 dB. The first of these three curves is what is expected assuming the simple, bistatic, first-power-law grazing-angle dependence when the geometry becomes increasingly vertically bistatic (given the fit constants derived for the less bistatic geometries). Note the physics-based model predictions are roughly 4 dB lower than this curve, providing better data matches over their full grazing angle range for this geometry, the most vertically bistatic (cf. Fig. 10).

### MF Results

Figures 29 and 30 correspond to the near-monostatic MF backscattering geometry where  $\theta_{scat} \approx 0.9 \cdot \theta_{inc}$ . Figure 29 shows a prediction of the scattering contribution due to the bottom interface. Key features include: a mild, monostatic frequency dependence; a dramatic null near 40 deg (due to shear effects); and a much more rapid falloff of BSS with decreasing grazing angle below  $\sim 20$  deg than seen in the acoustic data (cf. Fig. 18). Figure 30 shows the predicted effects of including a rockfish scattering contribution. In this case, the effect of the rockfish is quite small except at low grazing angles ( $< 10$  deg). Above 20 deg, the general levels of model curves match those of the data reasonably well (as corroborated by the thin model curve which represents a  $\mu$  of -25 dB). However, below 15 deg, the data levels are generally elevated (by up to 10 dB) over the predicted levels, suggesting the presence of a second, smaller fish species during the MF scattering measurements.

### Comments

As most of the geophysical and biological parameters were not directly measured, it should be noted that other choices of the parameter values could reproduce these data trends. The completion of the LWAD 99-3 volume scattering analysis [15] will help to set the biological parameter values with more confidence (at both LF and MF).

We also note that for angles above the p-wave critical angle of  $\sim 50$  deg, the physics-based, small-slope approximation predicts much stronger backscattering contributions from the water-sediment interface than does the empirical  $\mu + 10 \log(\sin \theta)$  formula, the differences increasing with increasing  $\theta$ .

<sup>9</sup>In this case only a third (or less) of the 46-m-thick fish layer is within the BSS receiver beams.

## SUMMARY

This report details the results of broadband, bistatic, direct-path measurements of bottom backscattering strength made during the Littoral Warfare Advanced Development 99-3 experiment, conducted in shallow water off the coast of Oregon in September 1999. Backscattering strengths were measured over 0.4 to 4.5 kHz for mean grazing angles of 4 to 40 degrees. In addition to the measured scattering results, empirical and physics-based model results are presented which provide insight into the local environmental acoustics.

At Site 1, all the acoustic data were fit adequately by assuming a first-power-law dependence of scattering strength on the sine of the mean grazing angle:  $\mu + 10 \log(\sin \theta)$  dB. For all geometries except the most vertically bistatic, scattering strengths for the LF band (400-1000 Hz) were well fit with  $\mu$ 's of -25 to -30 dB, while those in the MF band (1.5-4.5 kHz) were well fit with  $\mu$ 's of -20 to -30 dB. For the most vertically bistatic geometry, this formula (with  $\mu$ 's lowered by  $\sim 2.5$  dB) provided a good match generally only below 10 deg grazing. These results fall most closely into Group 2 (fine sand and silt bottoms) of McCammon's BSS model [8], which has a  $\mu$  interval of  $-27.5 \pm 6.8$  dB.

At the drifting site, LF scattering strengths can be approximated using  $\mu$ 's of -30 to -35 dB over the mean grazing angle range of 20 to 30 degrees. However, there was excessive array tilt during the only measurement sequence at this site. As array tilt violates the azimuthal symmetry of the measurement geometry, this likely produced measurement errors. Consequently, the data results from the drifting site should be treated with circumspection.

The physics-based, bistatic modeling results suggest that the dominant scattering mechanisms below  $\sim 50$  deg were the water-sediment interface and fish. At LF, the modeling suggested that rockfish in particular may have been a significant contributor at low grazing angles ( $< 20$  deg) to the LWAD 99-3 scattering strengths (even at relatively low densities). Additionally, at MF, a different and yet-undetermined (and un-modeled) fish species is likely contributing to the low-angle backscatter.

While the empirical formula  $\mu + 10 \log(\sin^{1/2} \theta_{inc} \cdot \sin^{1/2} \theta_{scat})$  generally provided a good fit to the measured backscattering strengths below 40 deg grazing, some caution should be taken in applying such formulas to general LWAD 99-3 multistatic performance assessments as: (1) these data all came from one site, and so represent only one of at least five distinct types of bottom material [14] that may have been encountered over the full 99-3 experimental area; (2) for the most vertically-bistatic data, the empirical formula only fit the data below 10 deg; and (3) for high grazing angles (above  $\sim 50$  deg at Site 1), the empirical formulas will seriously underpredict the contribution from the water-sediment interface. Furthermore, fish in shallow water can exhibit a high degree of variability, both spatially (range and depth) and temporally (e.g., day-vs-night), so that one can expect to see a corresponding variability acoustically. In particular, the behavior of backscattering strength in frequency and angle will be strongly dependent on the relative site-to-site abundances and varieties of fish.

## ACKNOWLEDGMENTS

This work was sponsored by the Office of Naval Research: the experiment and data processing/analysis by the *Littoral Warfare Advanced Development* Project, CDR Scott Tilden, Program Manager; and the modeling analysis by the *Multistatics Active Acoustics* Project, Roger Gauss, Project Manager. The authors thank Charles Thompson and Bob Fisher (NRL) for their at-sea assistance. The authors thank James Fulford and Redwood Nero (NRL) for providing geophysical and rockfish model inputs, respectively. The authors also thank Jerome Richardson, Lillian Fields, Joe Fialkowski, and Elisabeth Kim of Planning Systems, Incorporated, for assistance with the data processing.

## REFERENCES

1. R. J. Soukup and P. M. Ogden, "Bottom Backscattering Measured Off the South Carolina Coast During Littoral Warfare Advanced Development Focused Technology Experiment 96-2," NRL Memorandum Report 7140--97-7905, Naval Research Laboratory, Washington DC, April 28, 1997.
2. R. J. Soukup, "Bottom Backscattering Measured Off the Carolina Coast During Littoral Warfare Advanced Development System Concept Validation Experiment 97 (LWAD SCV 97)," NRL Formal Report 7140--98-9885, Naval Research Laboratory, Washington DC, June 15, 1998.
3. E. L. Kunz, "Bottom Backscattering Measured Off the Carolina Coast During Littoral Warfare Advanced Development 98-4 Experiment," NRL Memorandum Report 7140--98-8339, Naval Research Laboratory, Washington, DC, February 26, 1999.
4. R. J. Soukup and D. W. Edsall, "Bottom Backscattering Measured Southwest of Key West During Littoral Warfare Advanced Development Focused Technology Experiment 97-2," NRL Memorandum Report 7140--97-7977, Naval Research Laboratory, Washington, DC, September 30, 1997.
5. E. L. Kunz, "Bottom Backscattering Measured Off the Southwest Coast of Florida During the Littoral Warfare Advanced Development 98-2 Experiment," NRL Memorandum Report 7140--98-8196, Naval Research Laboratory, Washington, DC, September 4, 1998.
6. E. L. Kunz, "Bottom Backscattering Measured Off the Southwest Coast of Florida During the Littoral Warfare Advanced Development 99-1 Experiment," NRL Memorandum Report 7140--99-8389, Naval Research Laboratory, Washington, DC, July 30, 1999.
7. K. V. Mackenzie, "Bottom reverberation for 530 and 1030 cps sound in deep water," *J. Acoust. Soc. Am* **33**, 1498-1504 (1961).
8. D. F. McCammon, "Low Grazing Angle Bottom Scattering Strength: Survey of Unclassified Measurements and Models and Recommendations for LFA Use," *J. Underwater Acoust.* **43**, 33-47 (1993).
9. R. C. Gauss, D. Wurmser, R. W. Nero, and J. M. Fialkowski, "New Bistatic Models for Predicting Bottom, Surface, and Volume Scattering Strengths," Proceedings of the 28th Annual International Meeting of TTCP MAR TP-9 (1999).
10. C. H. Thompson, "LWAD 99-3 Quick Look Volume Scattering Measurements," LWAD 99-3 Quick Look Briefing, Arlington, VA, Oct 1999.
11. D. Wurmser, "A manifestly reciprocal theory of scattering in the presence of elastic media," *J. Math. Phys.* **37**, 4434-4479 (1996).

12. R. H. Love, "Resonant acoustic scattering by swimbladder-bearing fish," *J. Acoust. Soc. Am.* **64**, 571-580 (1978).
13. K. L. Williams and D. R. Jackson, "Bistatic bottom scattering: Model, experiments, and model/data comparison," *J. Acoust. Soc. Am.* **103**, 169-181 (1998).
14. J. K. Fulford, Naval Research Laboratory, Stennis Space Center, MS, personal communication (Feb 2000).
15. C. H. Thompson, R. W. Nero, and R. H. Love, "Volume Scattering on the Littoral Warfare Advanced Development 99-3 Experiment," NRL Memorandum Report in preparation, Naval Research Laboratory, Stennis Space Center, MS, 2000.

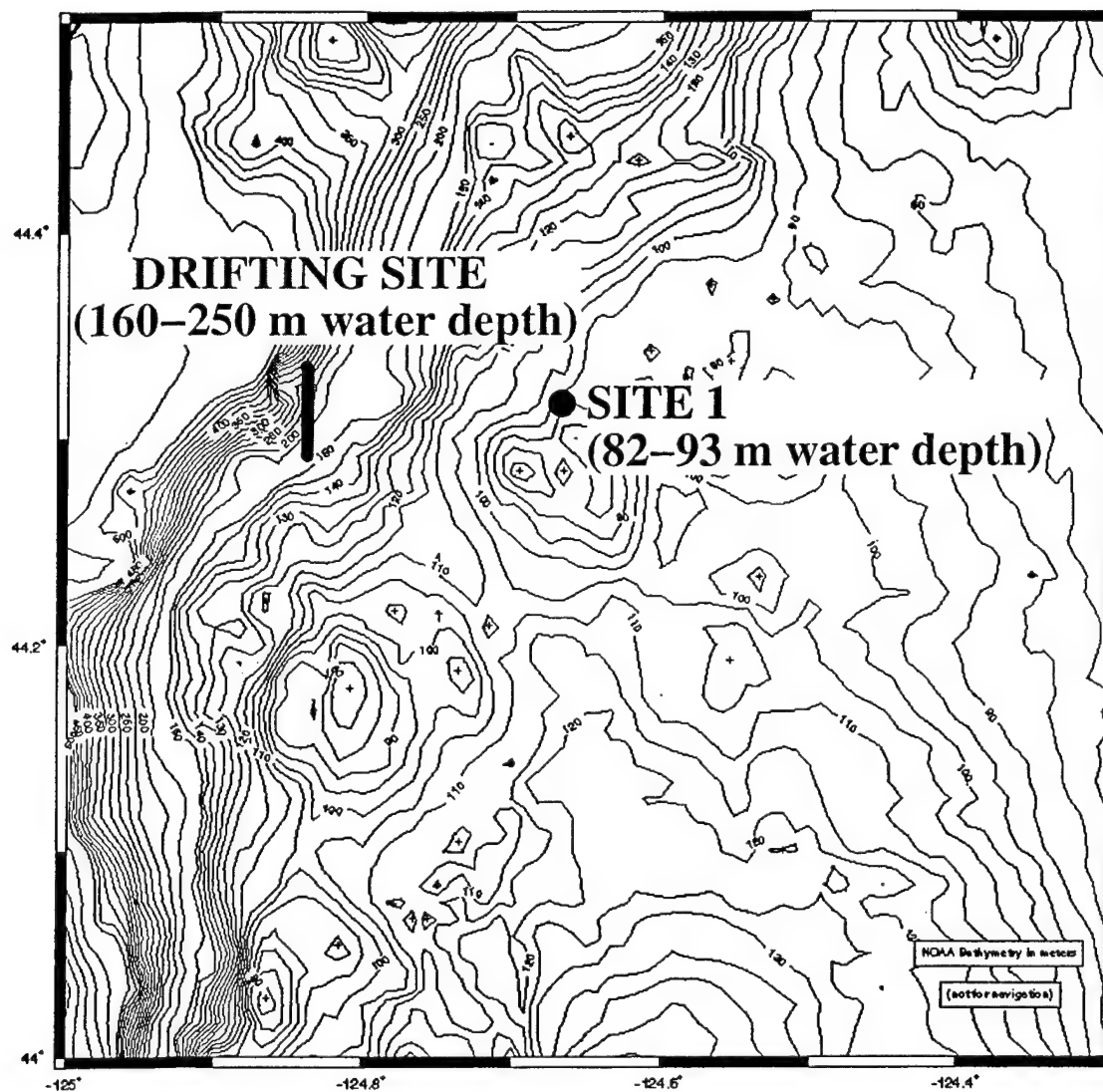


Fig. 1 — LWAD 99-3 bottom scattering sites. The water depth contours are measured in meters.

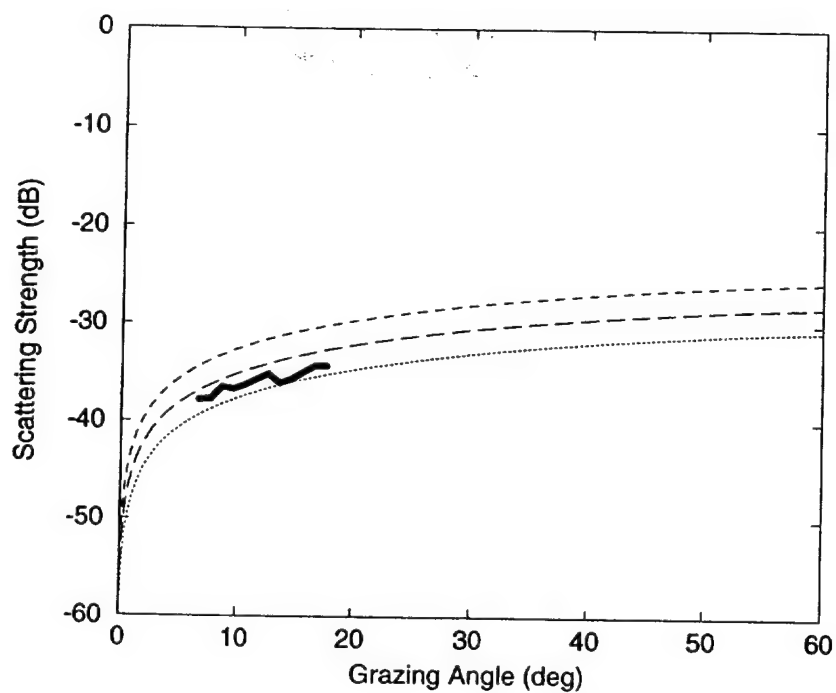


Fig. 2 — Near-monostatic bottom backscattering strength as a function of grazing angle for 400 Hz at Site 1. The dashed curves represent  $\mu + 10 \log(\sin \theta)$  for  $\mu = -25, -27.5$  and  $-30$  dB.

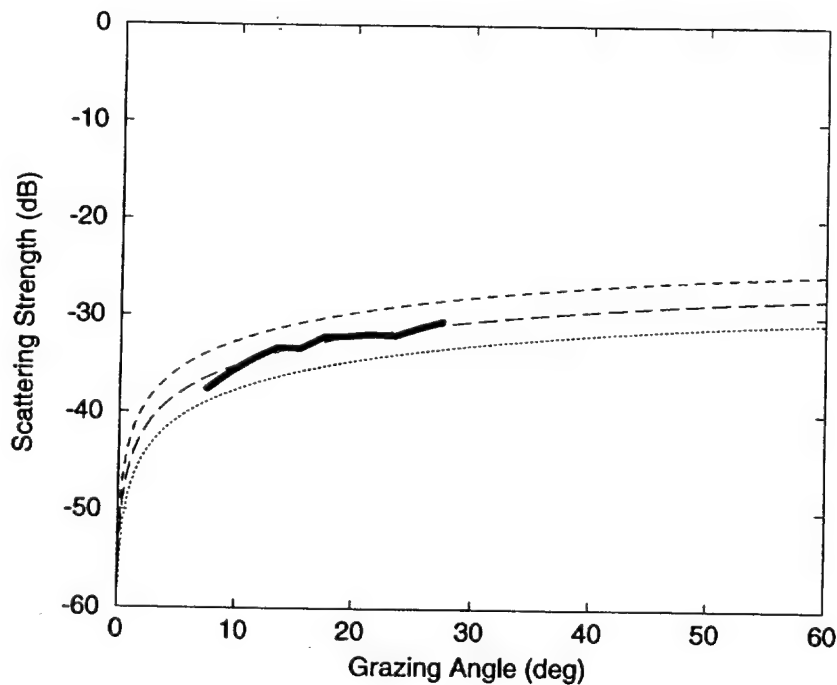


Fig. 3 — Near-monostatic bottom backscattering strength as a function of grazing angle for 600 Hz at Site 1. The dashed curves represent  $\mu + 10 \log(\sin \theta)$  for  $\mu = -25, -27.5$  and  $-30$  dB.

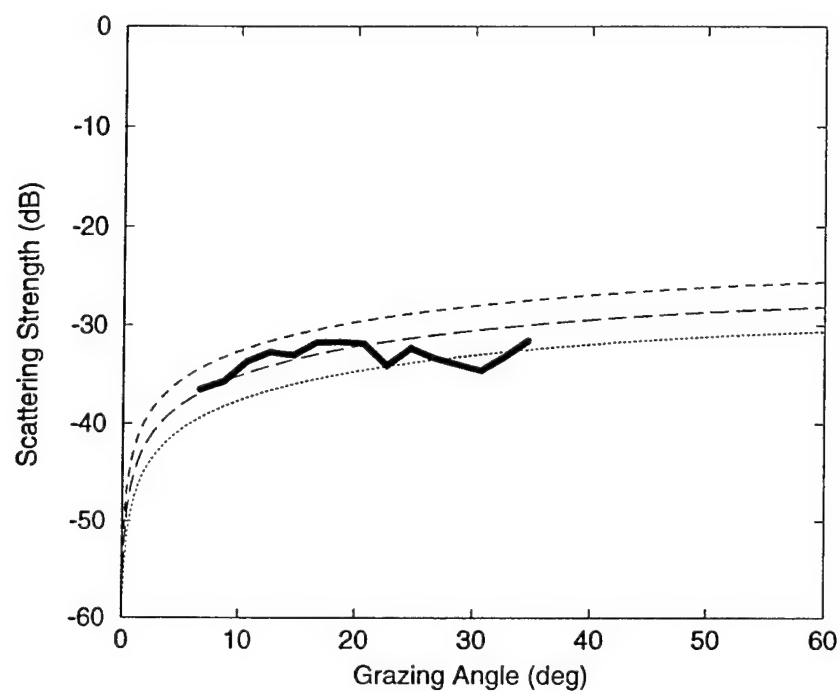


Fig. 4 — Near-monostatic bottom backscattering strength as a function of grazing angle for 800 Hz at Site 1. The dashed curves represent  $\mu + 10 \log(\sin \theta)$  for  $\mu = -25, -27.5$  and  $-30$  dB.

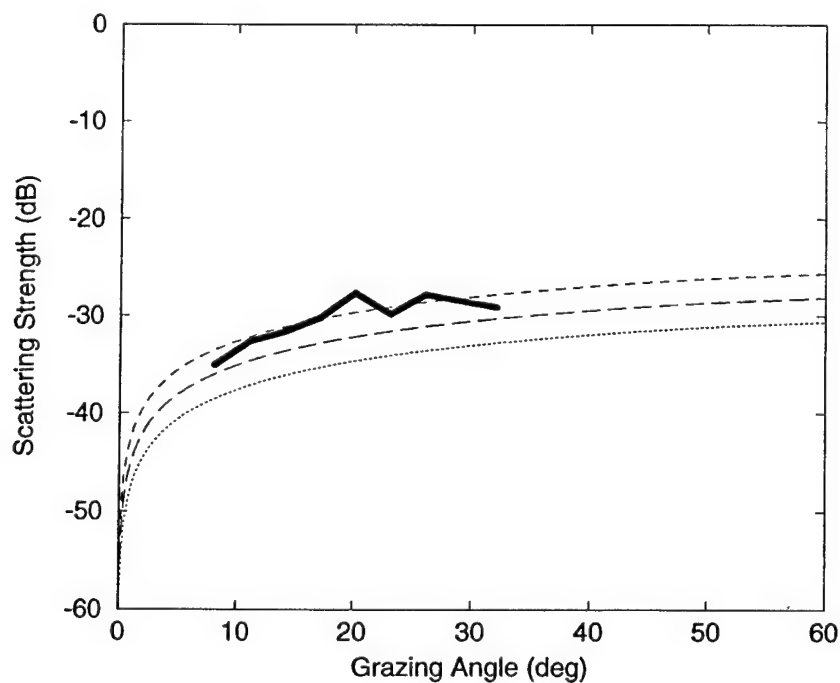


Fig. 5 — Near-monostatic bottom backscattering strength as a function of grazing angle for 1000 Hz at Site 1. The dashed curves represent  $\mu + 10 \log(\sin \theta)$  for  $\mu = -25, -27.5$  and  $-30$  dB.

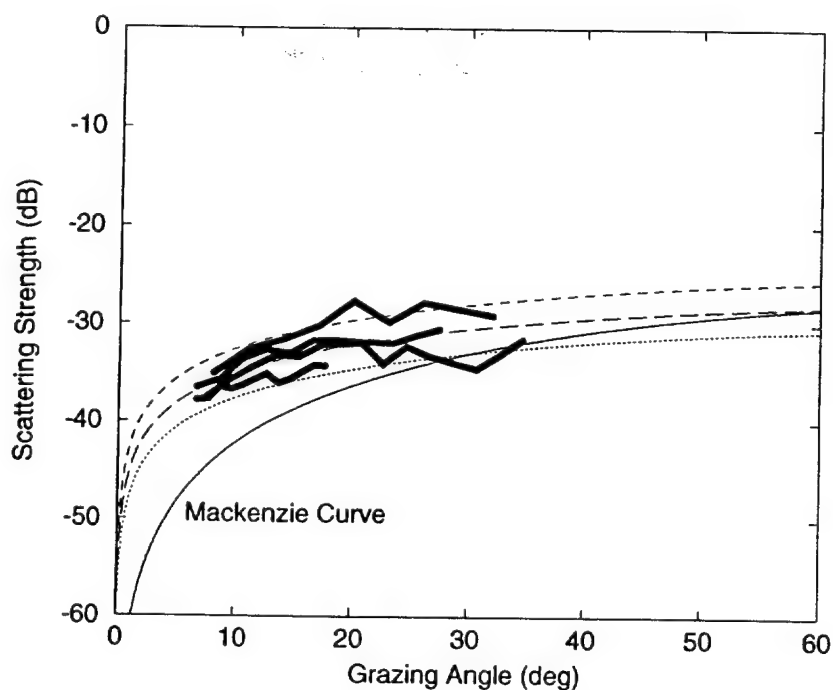


Fig. 6 — Near-monostatic bottom backscattering strength as a function of grazing angle for all LF frequencies (400, 600, 800, and 1000 Hz) at Site 1. The dashed curves represent  $\mu + 10 \log(\sin \theta)$  for  $\mu = -25, -27.5$  and  $-30$  dB. The Mackenzie curve is also shown.

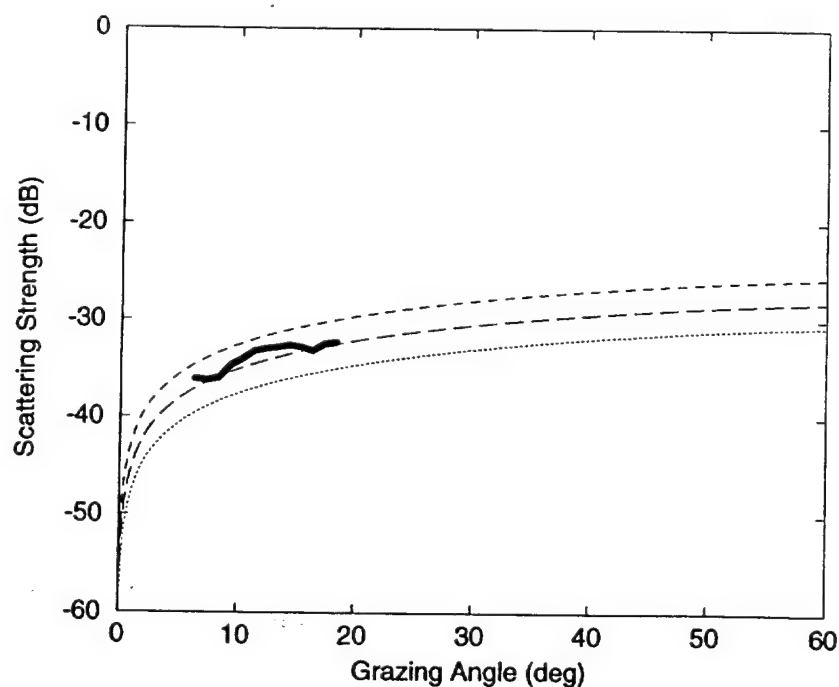


Fig. 7 — Near-monostatic bottom backscattering strength as a function of grazing angle for the low-frequency LFM signal (400-1000 Hz) at Site 1. The dashed curves represent  $\mu + 10 \log(\sin \theta)$  for  $\mu = -25, -27.5$  and  $-30$  dB.

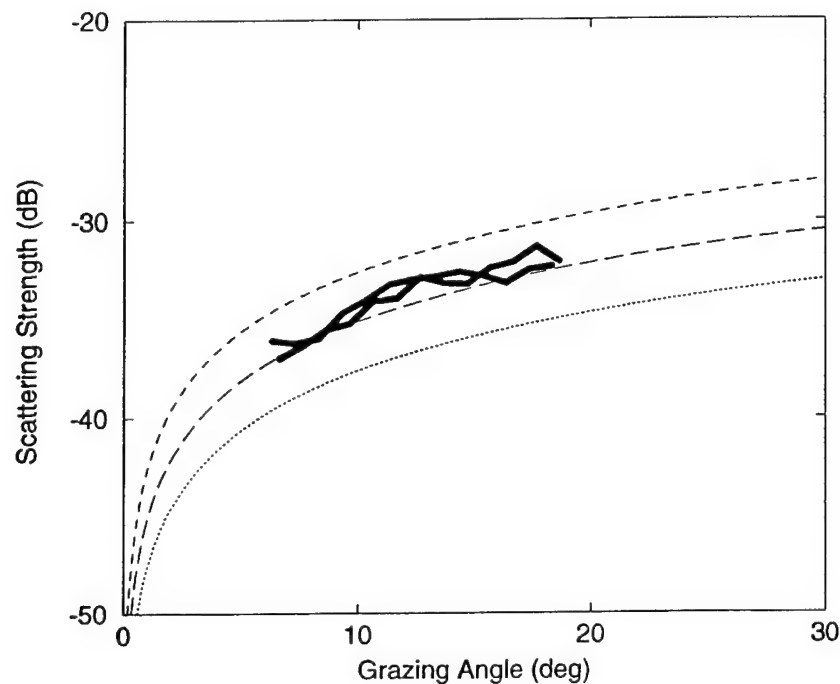


Fig. 8 — Near-monostatic bottom backscattering strength as a function of grazing angle averaged over the four LF frequencies shown in Fig. 6 compared to the bottom backscattering strength of the low-frequency LFM signal shown in Fig. 7. The dashed curves represent  $\mu + 10\log(\sin \theta)$  for  $\mu = -25, -27.5$  and  $-30$  dB.

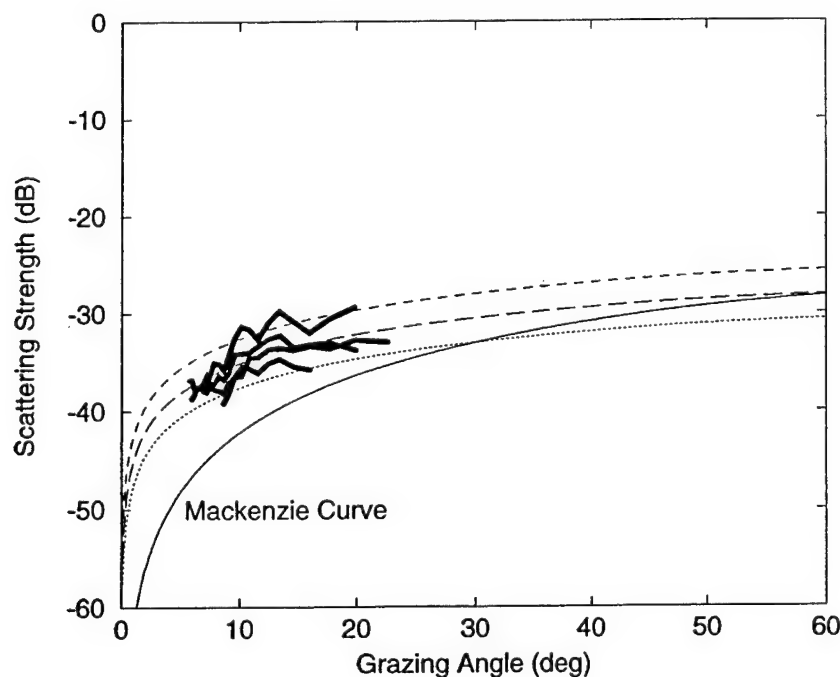


Fig. 9 — Vertically bistatic bottom backscattering strength as a function of grazing angle for the LF frequencies (400, 600, 800, and 1000 Hz) at Site 1. The source (at 21 m depth) and receiver (at 51 m depth) were separated by 30 m. The dashed curves represent  $\mu + 10\log(\sin \theta)$  for  $\mu = -25, -27.5$  and  $-30$  dB.

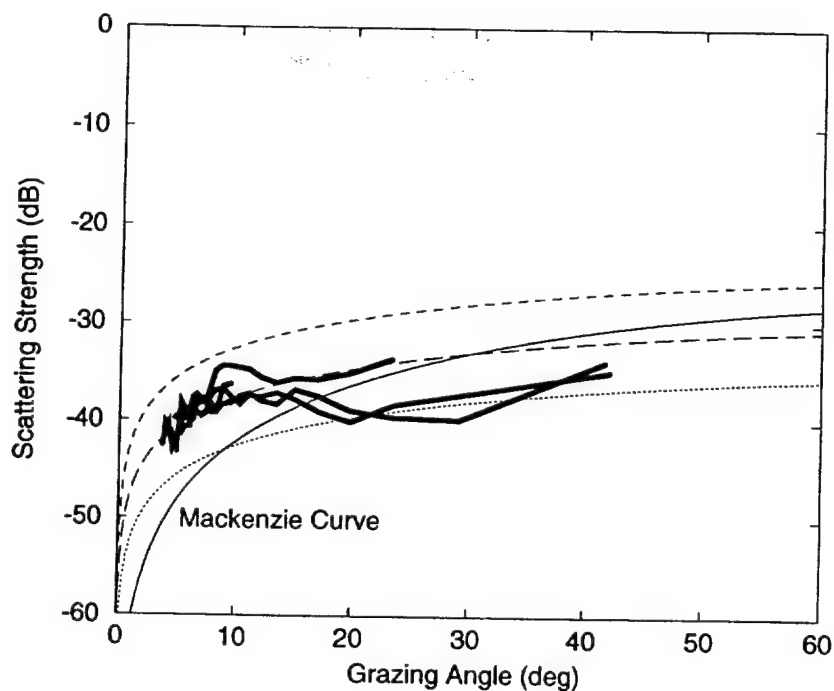


Fig. 10 — Vertically bistatic bottom backscattering strength as a function of grazing angle for the LF frequencies (400, 600, 800, and 1000 Hz) at Site 1. The source (at 21 m depth) and receiver (at 76 m depth) were separated by 55 m. The dashed curves represent  $\mu + 10 \log(\sin \theta)$  for  $\mu = -25, -30$  and  $-35$  dB.

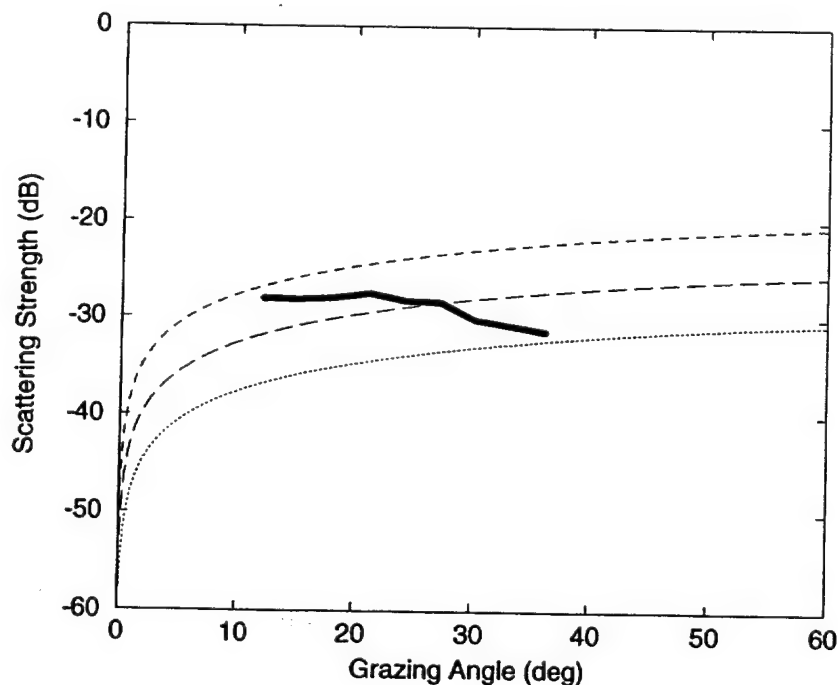


Fig. 11 — Near-monostatic bottom backscattering strength as a function of grazing angle for 1.5 kHz at Site 1. The dashed curves represent  $\mu + 10 \log(\sin \theta)$  for  $\mu = -20, -25$  and  $-30$  dB.

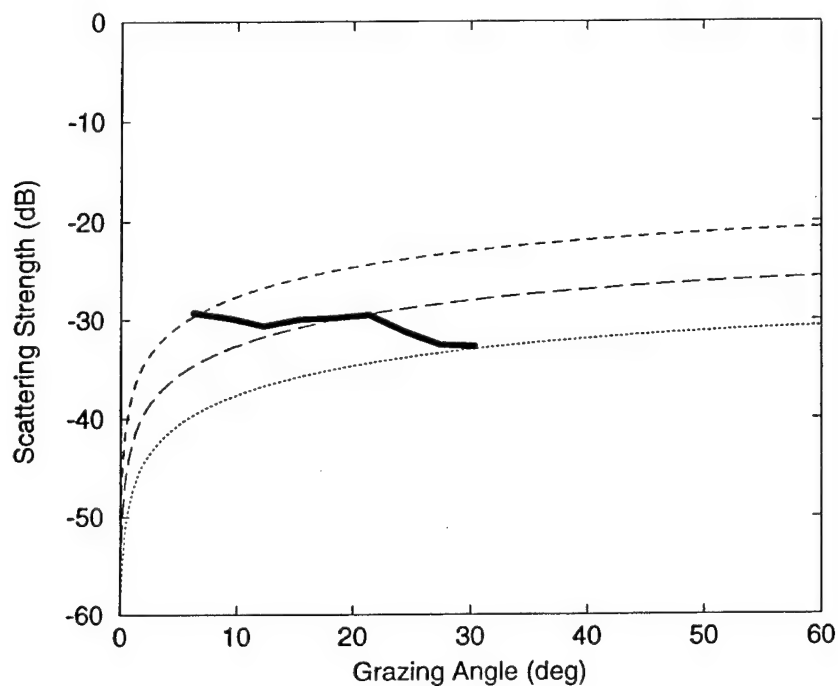


Fig. 12 — Near-monostatic bottom backscattering strength as a function of grazing angle for 2 kHz at Site 1. The dashed curves represent  $\mu + 10 \log(\sin \theta)$  for  $\mu = -20, -25$  and  $-30$  dB.

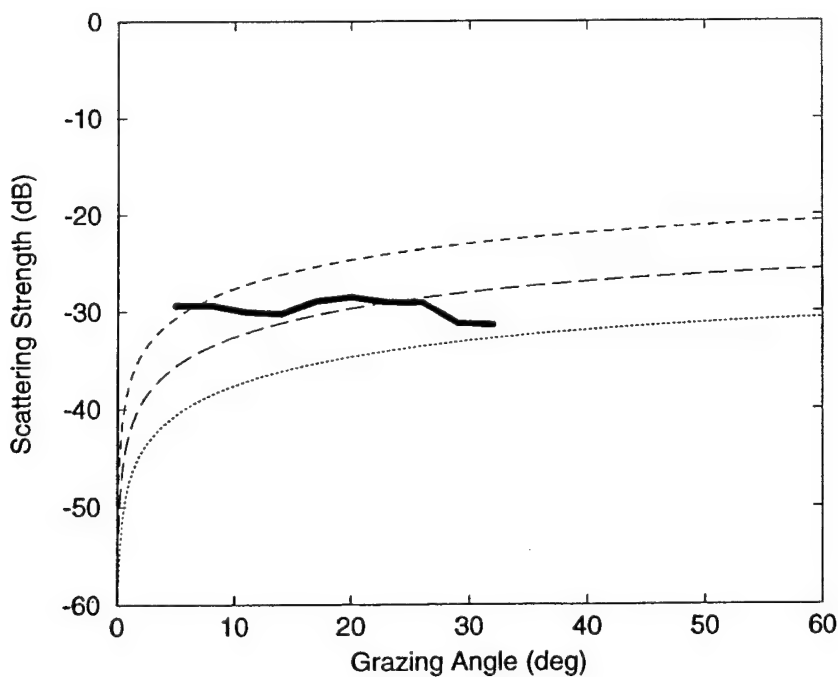


Fig. 13 — Near-monostatic bottom backscattering strength as a function of grazing angle for 2.5 kHz at Site 1. The dashed curves represent  $\mu + 10 \log(\sin \theta)$  for  $\mu = -20, -25$  and  $-30$  dB.

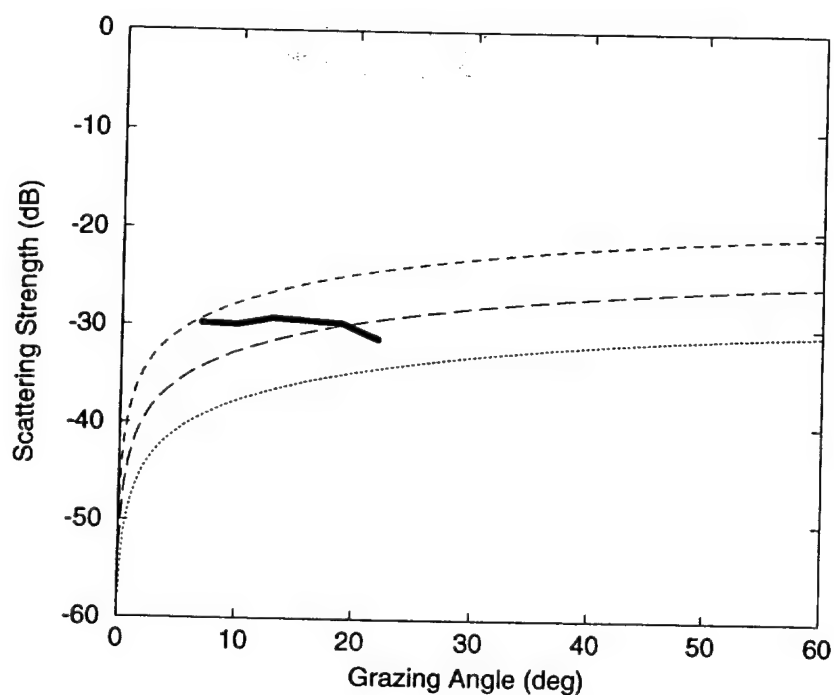


Fig. 14 — Near-monostatic bottom backscattering strength as a function of grazing angle for 3 kHz at Site 1. The dashed curves represent  $\mu + 10 \log(\sin \theta)$  for  $\mu = -20, -25$  and  $-30$  dB.

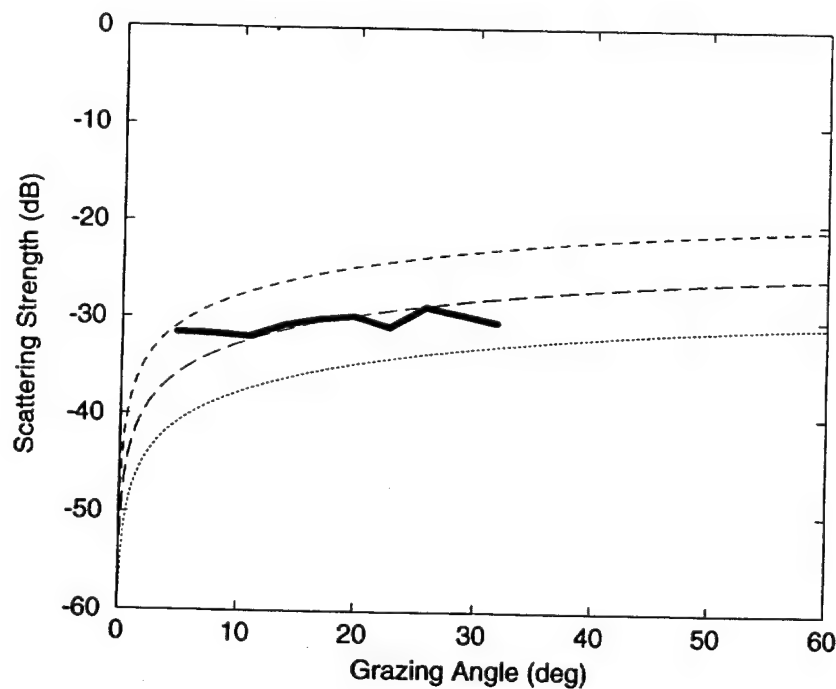


Fig. 15 — Near-monostatic bottom backscattering strength as a function of grazing angle for 3.5 kHz at Site 1. The dashed curves represent  $\mu + 10 \log(\sin \theta)$  for  $\mu = -20, -25$  and  $-30$  dB.

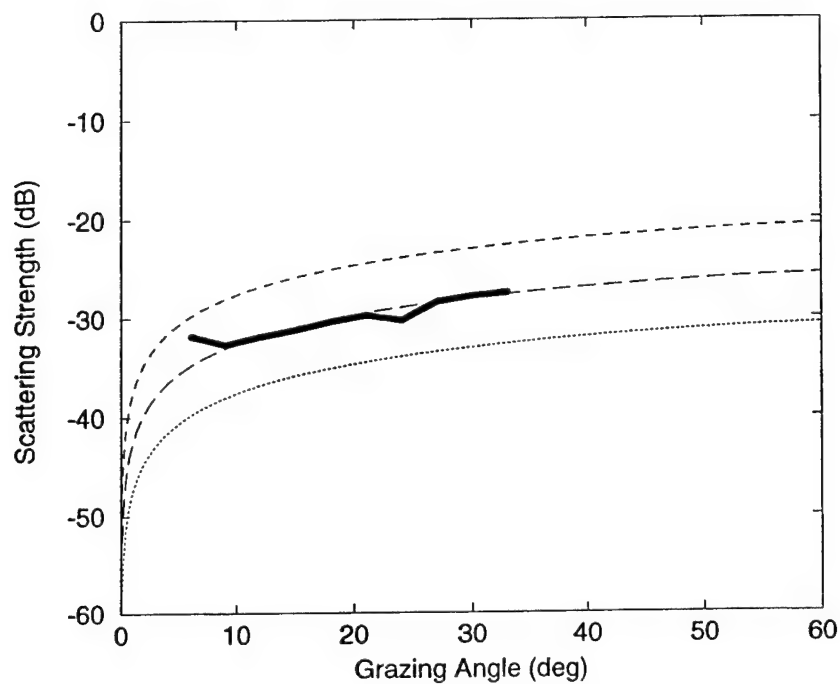


Fig. 16 — Near-monostatic bottom backscattering strength as a function of grazing angle for 4 kHz at Site 1. The dashed curves represent  $\mu + 10 \log(\sin \theta)$  for  $\mu = -20, -25$  and  $-30$  dB.

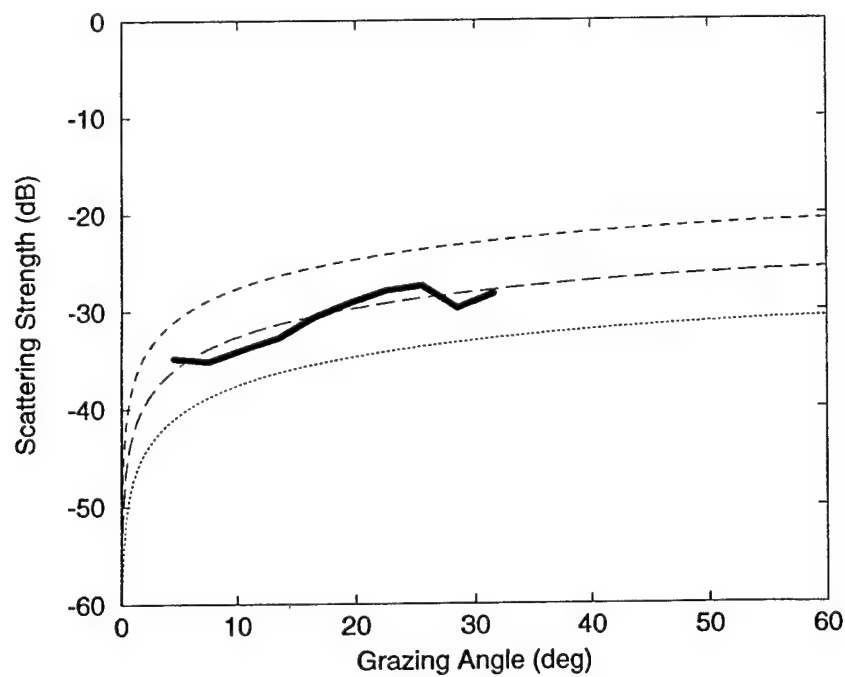


Fig. 17 — Near-monostatic bottom backscattering strength as a function of grazing angle for 4.5 kHz at Site 1. The dashed curves represent  $\mu + 10 \log(\sin \theta)$  for  $\mu = -20, -25$  and  $-30$  dB.

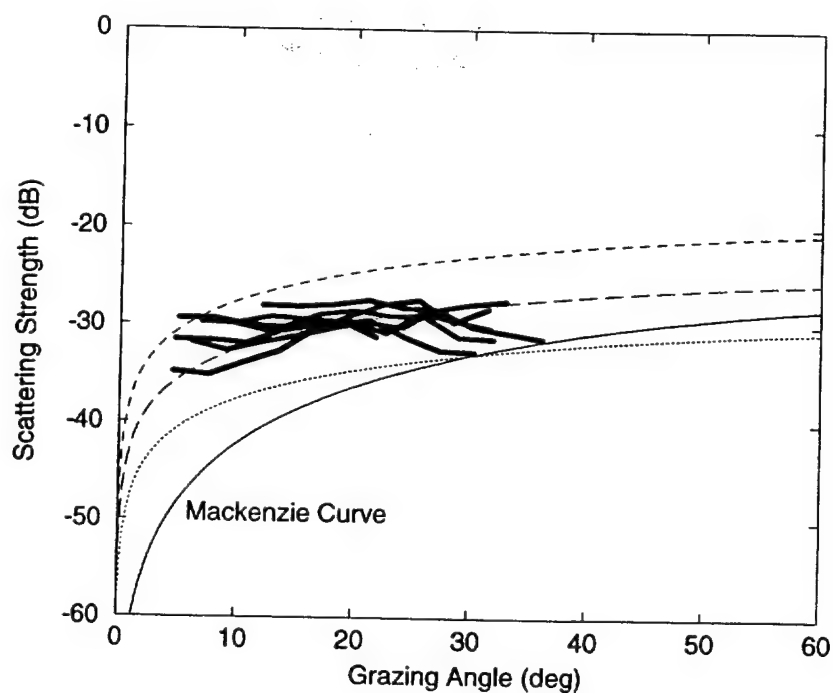


Fig. 18 — Near-monostatic bottom backscattering strength as a function of grazing angle for all MF frequencies (1.5, 2, 2.5, 3, 3.5, 4, and 4.5 kHz) at Site 1. The dashed curves represent  $\mu + 10 \log(\sin \theta)$  for  $\mu = -20, -25$  and  $-30$  dB. The Mackenzie curve is also shown.

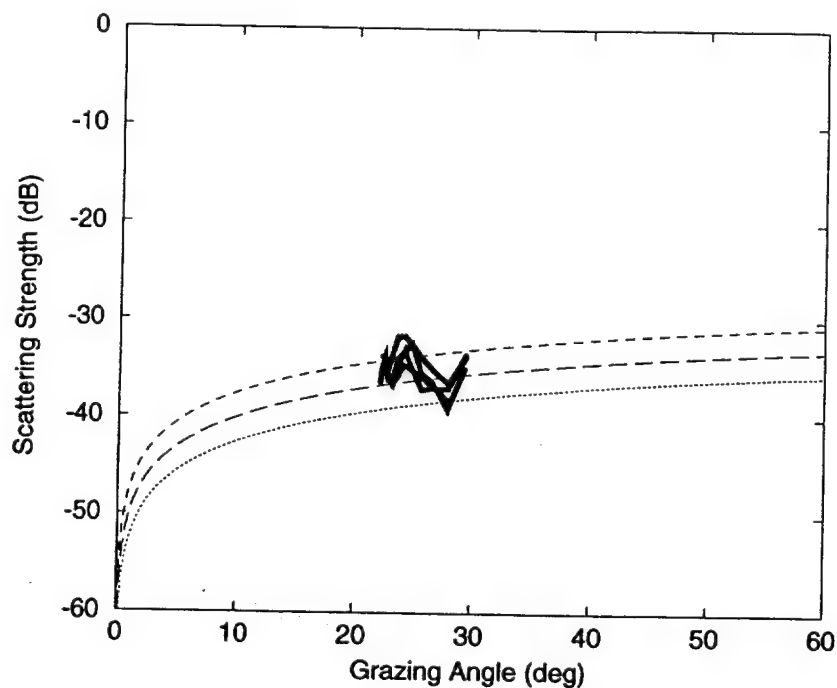


Fig. 19 — Near-monostatic bottom backscattering strength as a function of grazing angle for all LF frequencies (400, 600, 800, and 1000 Hz) at the drifting site. The dashed curves represent  $\mu + 10 \log(\sin \theta)$  for  $\mu = -30, -32.5$  and  $-35$  dB.

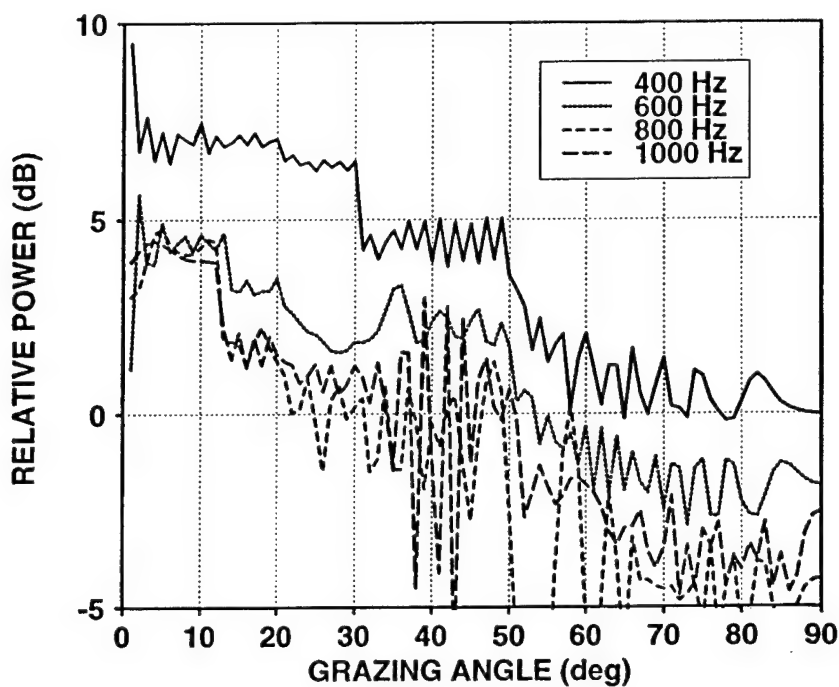


Fig. 20 — Difference of monostatic model predictions of rockfish backscattering strength as a function of grazing angle for the four LF frequencies. The difference represents including, minus not including, bottom-interference effects.

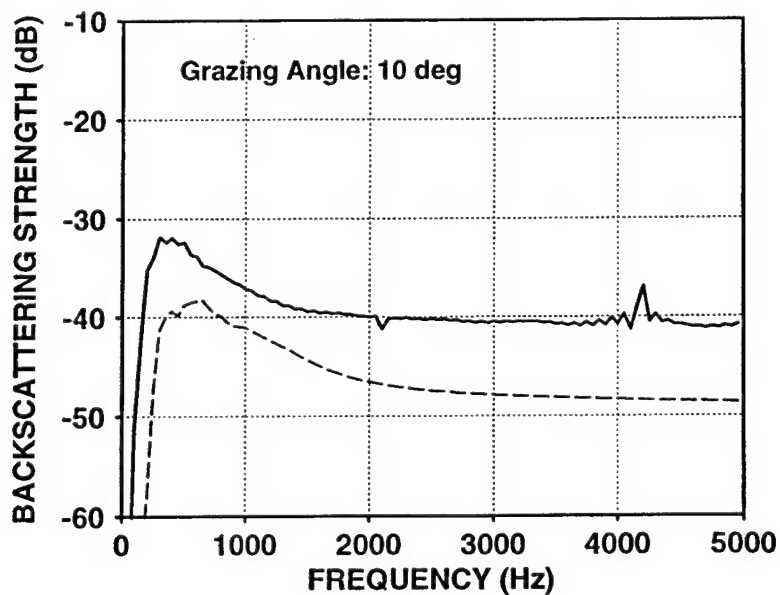


Fig. 21 — Modeled monostatic backscattering strength as a function of frequency due to rockfish for the four LF frequencies at a nominal low grazing angle. The two predictions reflect including (solid curve) and excluding (dashed curve) bottom-interference effects in the modeling.

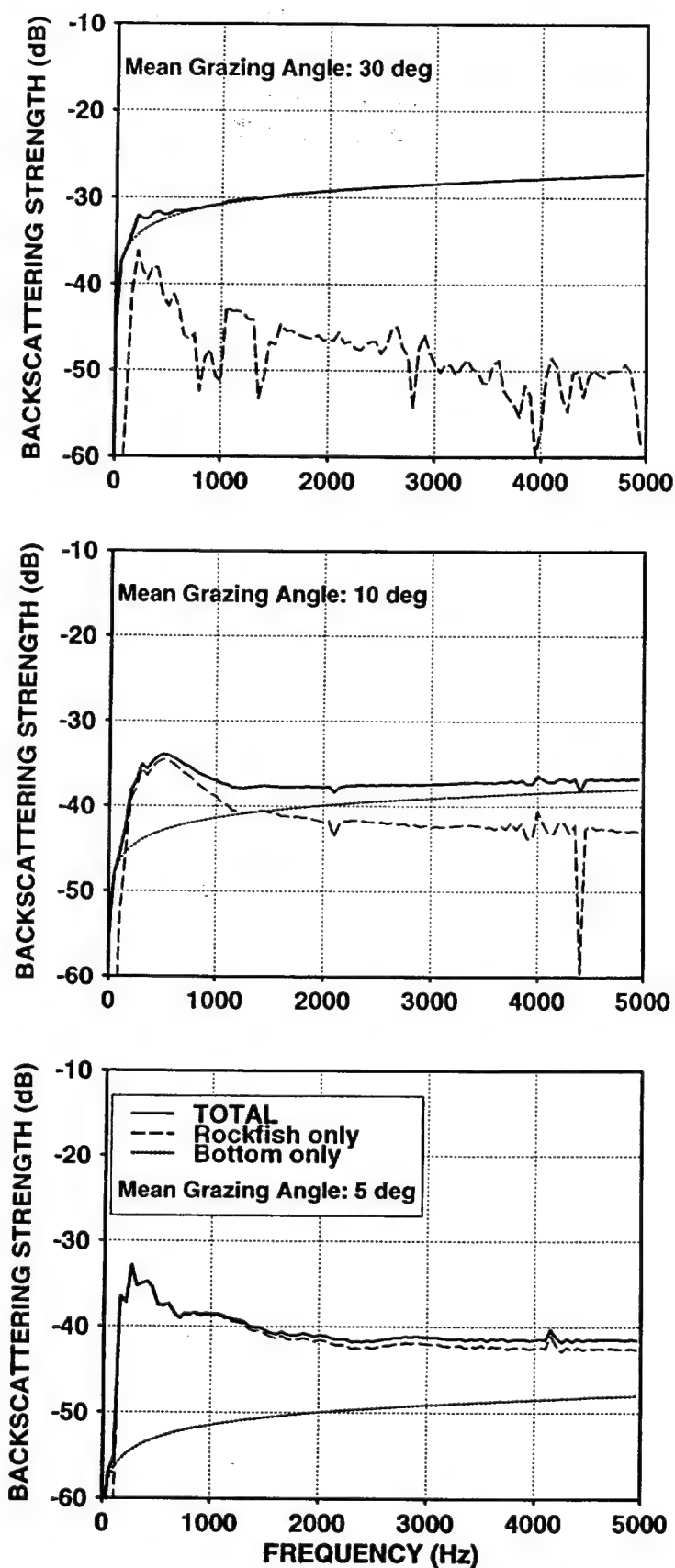


Fig. 22 — Modeled near-monostatic ( $\theta_{scat} = 0.9 \cdot \theta_{inc}$ ) backscattering strength as a function of frequency for the water-sediment interface only (dotted curves), rockfish only (dashed curves), and the combination of both effects (solid curves), at three mean grazing angles: (top) 30 deg; (middle) 10 deg; (bottom) 5 deg.

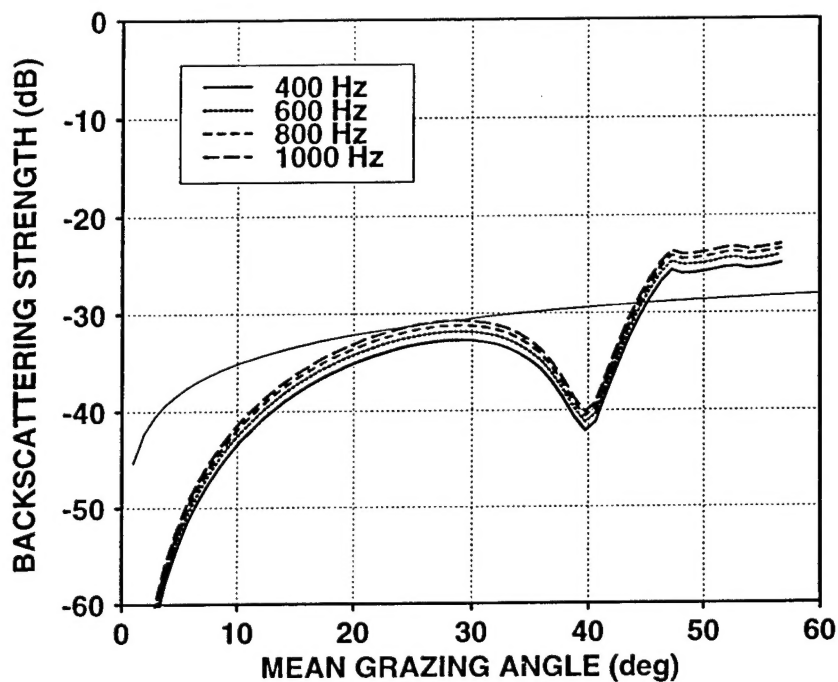


Fig. 23 — Modeled near-monostatic ( $\theta_{scat} = 0.9 \cdot \theta_{inc}$ ) backscattering strength as a function of mean grazing angle due to scattering from the water-sediment interface only for the four LF frequencies. The thin solid curve represents  $\mu + 10 \log(\sin^{1/2} \theta_{inc} \cdot \sin^{1/2} \theta_{scat})$  for  $\mu = -27.5$  dB.

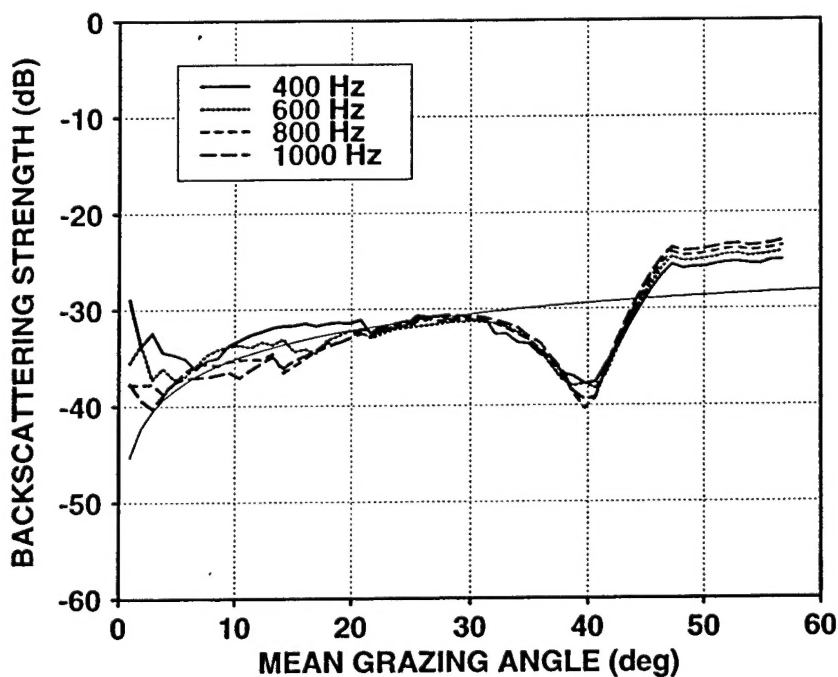


Fig. 24 — Modeled near-monostatic ( $\theta_{scat} = 0.9 \cdot \theta_{inc}$ ) backscattering strength as a function of mean grazing angle due to the combination of scattering from the water-sediment interface and rockfish for the four LF frequencies. The thin solid curve represents  $\mu + 10 \log(\sin^{1/2} \theta_{inc} \cdot \sin^{1/2} \theta_{scat})$  for  $\mu = -27.5$  dB.

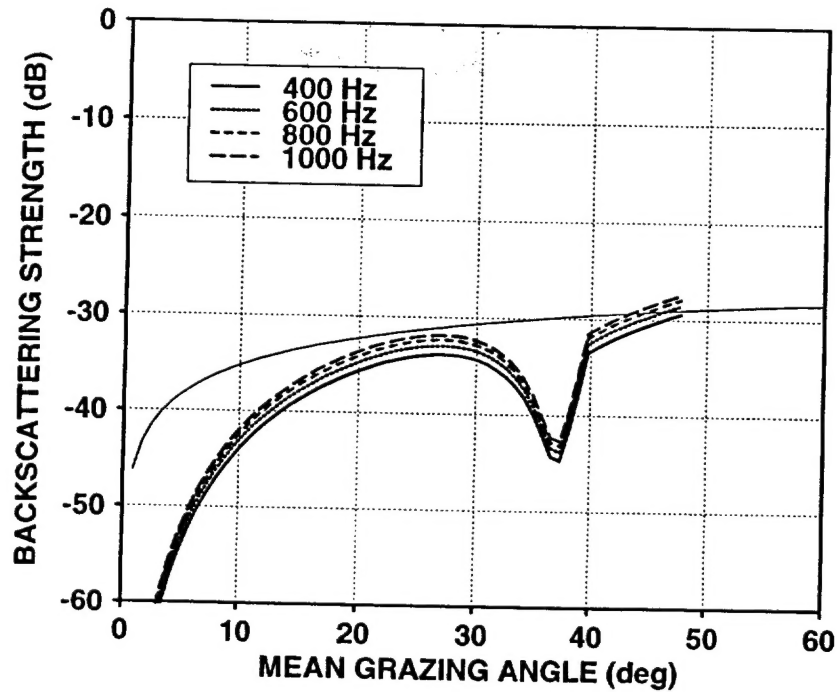


Fig. 25 — Modeled bistatic ( $\theta_{scat} = 0.6 \cdot \theta_{inc}$ ) backscattering strength as a function of mean grazing angle due to scattering from the water-sediment interface only for the four LF frequencies. The thin solid curve represents  $\mu + 10 \log(\sin^{1/2} \theta_{inc} \cdot \sin^{1/2} \theta_{scat})$  for  $\mu = -27.5$  dB.

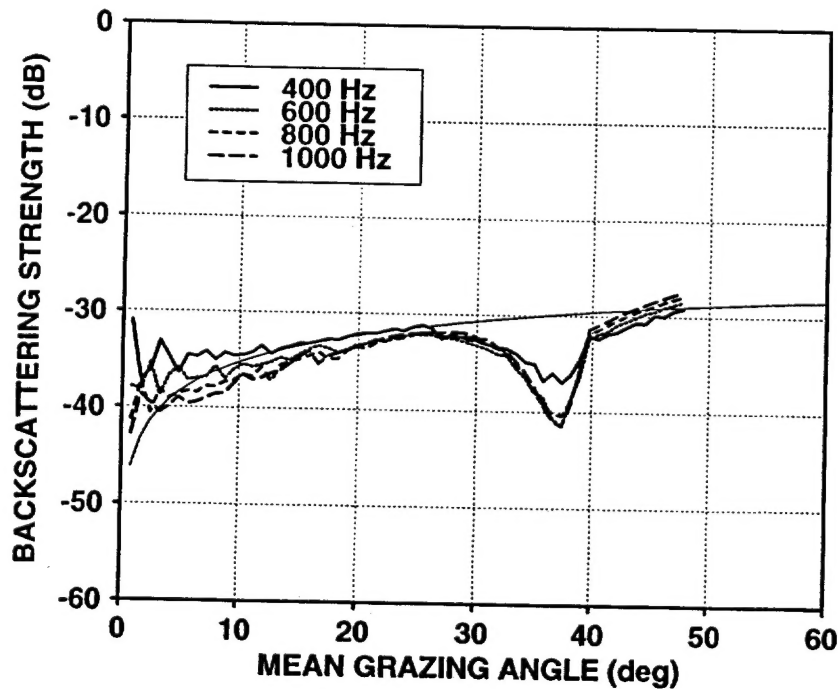


Fig. 26 — Modeled bistatic ( $\theta_{scat} = 0.6 \cdot \theta_{inc}$ ) backscattering strength as a function of mean grazing angle due to the combination of scattering from the water-sediment interface and rockfish for the four LF frequencies. The thin solid curve represents  $\mu + 10 \log(\sin^{1/2} \theta_{inc} \cdot \sin^{1/2} \theta_{scat})$  for  $\mu = -27.5$  dB.

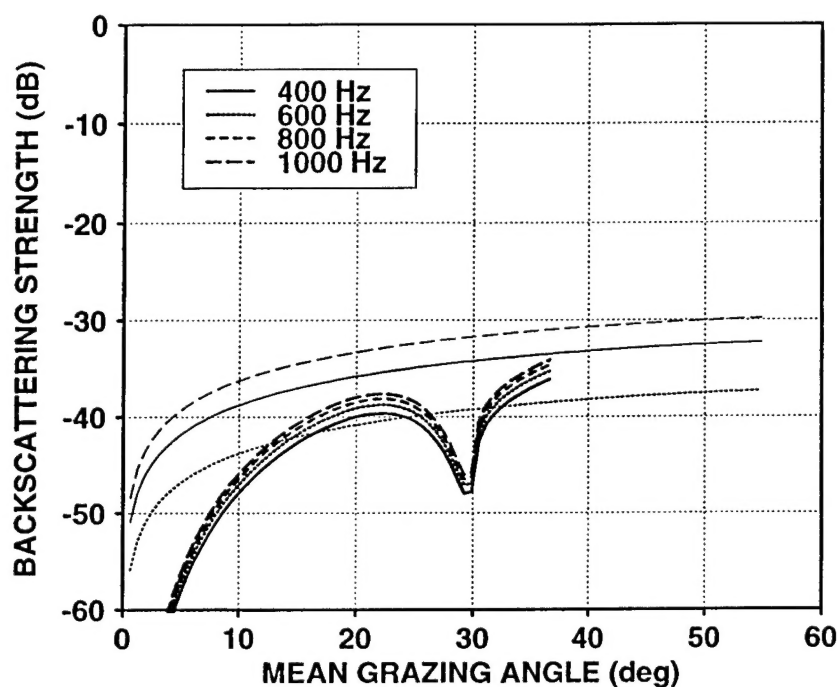


Fig. 27 — Modeled bistatic ( $\theta_{scat} = 0.2 \cdot \theta_{inc}$ ) backscattering strength as a function of mean grazing angle due to scattering from the water-sediment interface only for the four LF frequencies. The thin dashed, solid and dotted curves represent  $\mu + 10 \log(\sin^{1/2} \theta_{inc} \cdot \sin^{1/2} \theta_{scat})$  for  $\mu = -27.5, -30$  and  $-35$  dB, respectively.

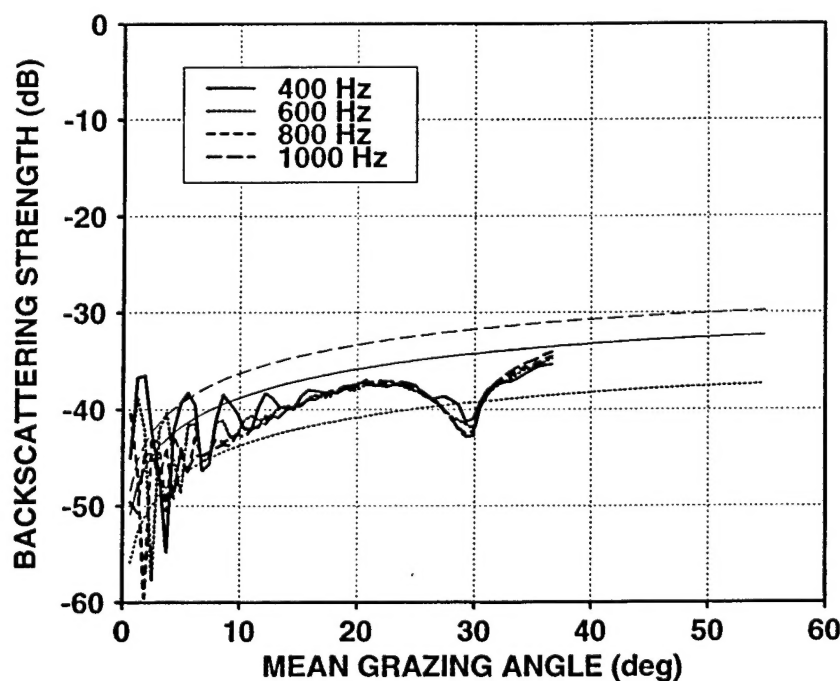


Fig. 28 — Modeled bistatic ( $\theta_{scat} = 0.2 \cdot \theta_{inc}$ ) backscattering strength as a function of mean grazing angle due to the combination of scattering from the water-sediment interface and rockfish for the four LF frequencies. The thin dashed, solid and dotted curves represent  $\mu + 10 \log(\sin^{1/2} \theta_{inc} \cdot \sin^{1/2} \theta_{scat})$  for  $\mu = -27.5, -30$  and  $-35$  dB, respectively.

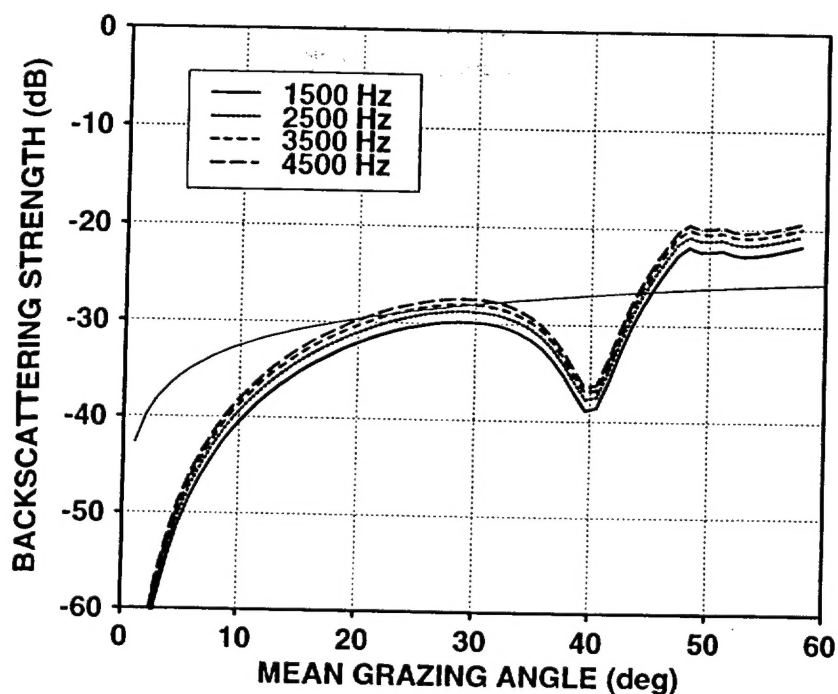


Fig. 29 — Modeled near-monostatic ( $\theta_{scat} = 0.9 \cdot \theta_{inc}$ ) backscattering strength as a function of mean grazing angle due to scattering from the water-sediment interface only for four MF frequencies. The thin solid curve represents  $\mu + 10 \log(\sin^{1/2} \theta_{inc} \cdot \sin^{1/2} \theta_{scat})$  for  $\mu = -25$  dB.

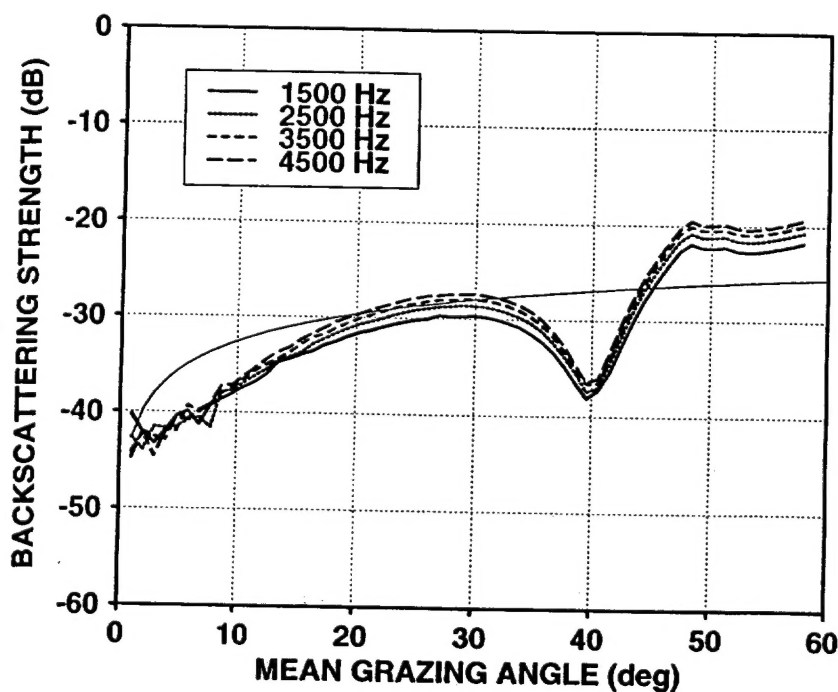


Fig. 30 — Modeled near-monostatic ( $\theta_{scat} = 0.9 \cdot \theta_{inc}$ ) backscattering strength as a function of mean grazing angle due to the combination of scattering from the water-sediment interface and rockfish for four MF frequencies. The thin solid curve represents  $\mu + 10 \log(\sin^{1/2} \theta_{inc} \cdot \sin^{1/2} \theta_{scat})$  for  $\mu = -25$  dB.